The Astronomical Journal, 132:692–710, 2006 August

THE ORBITS OF SATURN'S SMALL SATELLITES DERIVED FROM COMBINED HISTORIC AND *CASSINI* IMAGING OBSERVATIONS

J. N. Spitale
CICLOPS, Space Science Institute, 4750 Walnut Street, Suite 205, Boulder, CO 80301; spitale@lpl.arizona.edu

R. A. Jacobson
Jet Propulsion Laboratory, California Institute of Technology, 4800 Oak Grove Drive, Pasadena, CA 91109-8099

C. C. Porco
CICLOPS, Space Science Institute, 4750 Walnut Street, Suite 205, Boulder, CO 80301

AND

W. M. Owen, Jr.
Jet Propulsion Laboratory, California Institute of Technology, 4800 Oak Grove Drive, Pasadena, CA 91109-8099
Received 2006 February 28; accepted 2006 April 12

ABSTRACT

We report on the orbits of the small, inner Saturnian satellites, either recovered or newly discovered in recent *Cassini* imaging observations. The orbits presented here reflect improvements over our previously published values in that the time base of *Cassini* observations has been extended, and numerical orbital integrations have been performed in those cases in which simple precessing elliptical, inclined orbit solutions were found to be inadequate. Using combined *Cassini* and *Voyager* observations, we obtain an eccentricity for Pan 7 times smaller than previously reported because of the predominance of higher quality *Cassini* data in the fit. The orbit of the small satellite (S/2005 S1 [Daphnis]) discovered by *Cassini* in the Keeler gap in the outer A ring appears to be circular and coplanar; no external perturbations are apparent. Refined orbits of Atlas, Prometheus, Pandora, Janus, and Epimetheus are based on *Cassini* , *Voyager*, *Hubble Space Telescope*, and Earth-based data and a numerical integration perturbed by all the massive satellites and each other. Atlas is significantly perturbed by Prometheus, and to a lesser extent by Pandora, through high-wavenumber mean-motion resonances. Orbital integrations involving Atlas yield a mass of $GM_{\rm Atlas} = (0.44 \pm 0.04) \times 10^{-3}$ km^3 s^{-2}, 3 times larger than reported previously (GM is the product of the Newtonian constant of gravitation G and the satellite mass M). Orbital integrations show that Methone is perturbed by Mimas, Pallene is perturbed by Enceladus, and Polydeuces librates around Dione's L5 point with a period of about 791 days. We report on the nature and orbits of bodies sighted in the F ring, two of which may have persisted for a year or more.

Key words: planets: rings — planets and satellites: individual (Atlas, Daphnis, Epimetheus, Janus, Methone, Pallene, Pan, Pandora, Polydeuces, Prometheus)

Online material: machine-readable table

1. INTRODUCTION

Among the major objectives of the *Cassini* Imaging Subsystem (ISS) investigations at Saturn are the search for new Saturnian satellites, the accurate determination of the orbits of any newly discovered bodies, and the refinement of the orbits of the previously known Saturnian satellites. The greater sensitivity of the ISS cameras compared to those on the *Voyager* spacecraft (Porco et al. 2004), as well as the geometry and duration of the *Cassini* tour of the Saturn system, have already resulted in the discovery of satellites several times smaller than Pan and Atlas, the smallest discovered by *Voyager*. The purpose of this paper is to report the latest orbital elements for Pan, the newly discovered Keeler gap satellite S/2005 S1 (provisionally named Daphnis), Atlas, the F-ring shepherds Prometheus and Pandora, the F-ring "objects" S/2004 S3 and S/2004 S6, the "co-orbital" satellites Janus and Epimetheus, the newly discovered satellites found within the main satellite system Methone and Polydeuces, and the recovered satellite Pallene. We also describe the orbit determination procedures followed in the analyses of their motions and report here the details of the many *Cassini* observations that have been used in this work. The orbits for objects that were treated in Porco et al. (2005) are updated in this work using the most current *Cassini* images and the latest spacecraft trajectories. The orbits for Methone and Pallene are now based on orbital integrations that include the major perturbations in the Saturnian system. The Methone analysis has led to a better GM value for Mimas (Jacobson et al. 2006), which has allowed the orbits for Atlas, Prometheus, Pandora, Janus, and Epimetheus to be determined in a single integration (GM is the product of the Newtonian constant of gravitation G and the satellite mass M).

2. OBSERVATIONS AND DATA REDUCTION

The observations used in the orbit analyses presented here came from a variety of sources. Obviously, for the objects actually discovered by *Cassini*, the sole source of information was *Cassini* imaging data. For Pan and Pallene, images acquired by both *Cassini* and *Voyager 2* were used; for Atlas, Prometheus, Pandora, Janus, and Epimetheus, observations from *Cassini*, the *Hubble Space Telescope* (*HST*), ground-based telescopes, and *Voyager* were used (see § 5.3). For each satellite, Table 1 gives the source of the measurements. Table 3 (an unabridged version of which is available in the online supplement) lists the *Cassini* observational information collected from each image used in this work. The analyses presented here have used the most complete set of observations,

TABLE 1
SOURCES OF ALL OBSERVATIONS USED IN THIS WORK

Satellite	Type	References
Janus	Earth-based	1, 5, 6, 7, 8, 11
	HST	2, 3, 4
	Voyager 1 and *2*	
	Cassini	
Epimetheus	Earth-based	1, 5, 6, 7, 11
	HST	2, 3, 4
	Voyager 1 and *2*	
	Cassini	
Atlas	*HST*	4
	Voyager 1 and *2*	
	Cassini	
Prometheus	Earth-based	6, 7, 8, 11
	HST	2, 3, 4
	Voyager 1 and *2*	
	Cassini	
Pandora	Earth-based	6
	HST	2, 3, 4
	Voyager 1 and *2*	
	Cassini	
Pan	*Voyager 2*	9
	Cassini	
Methone (S/2004 S1)	*Cassini*	
Pallene (S/2004 S2)	*Voyager 2*	10
	Cassini	
Polydeuces (S/2004 S5)	*Cassini*	
Daphnis (S/2005 S1)	*Cassini*	

REFERENCES.—(1) Dollfus & Brunier 1981; (2) R. G. French 2001, private communication (*HST* observations: 1994 December 1 to 1995 November 18); (3) French et al. 2006; (4) McGhee et al. 2001; (5) Nicholson et al. 1992; (6) F. Poulet & B. Sicardy 2001, private communication; (7) Seidelmann et al. 1981; (8) Sharringhausen et al. 2003; (9) Showalter 1991; (10) Synnott 1986; (11) Yoder et al 1989.

both historic and new, available for these objects as of the dates given in Table 2.

2.1. *Point-Source Measurements on Cassini Images*

Cassini images were navigated (i.e., accurate celestial pointing of the camera was determined; see below) to determine accurate celestial coordinates of the satellites. For navigation purposes, it was necessary to determine the locations of stars in the image. For satellite orbital analyses, it was necessary to determine the location of the satellites, some images of which were unresolved. Locating stars and unresolved satellites involves the measurement of the positions of point-source images.

Point-source positions were measured by finding the best correlation between a Gaussian point-spread model and a subregion of the image surrounding the source to be measured. Subpixel precision was obtained by fitting the correlation peak to a Gaussian profile and taking the best-fitting center as the object's location. Point-spread full widths at half-maxima for the narrow-angle camera (NAC) and wide-angle camera (WAC) were taken as 1.3 and 1.8 pixels, respectively (Porco et al. 2004). Although recent work has shown that the point-spread function (PSF) is not accurately represented by a Gaussian, the center of a best-fit Gaussian is a good estimate of the center of the PSF, because the PSF is highly symmetric (in both the NAC and WAC). For smeared point sources we estimated the midpoint of the streak by eye, as the times of the midpoints of the exposures were used for all of our calculations.

In the case of Pallene, which we show below is the same object as 1981 S14 first observed by *Voyager 2*, we reanalyzed the single *Voyager* image of that body. In addition to the other steps described in this work, it was necessary in this image to correct for the significant distortions inherent in the selenium-sulfur Vidicon detector by comparing the fiducial "reseau" marks to their known focal-plane locations (Danielson et al. 1981).

2.2. *Pointing and Trajectory Corrections*

Images were navigated by fitting the computed positions of catalog stars to their measured image positions. We used a merged star catalog containing 48,767,342 stars, of which 436,771 (mostly bright) are from Tycho-2 only, 46,216,371 are from UCAC-2 (USNO CCD Astrographic Catalog 2) only, and 2,114,200 are in both catalogs. Common stars take their positions and proper motions from UCAC-2, while the other information is from Tycho-2. Magnitudes of Tycho-2 stars are corrected to the *Cassini* clear filter passband, and magnitudes of UCAC-2 stars are already somewhere between V and R.

Because the stars are extremely far away, pointing corrections obtained using stellar locations are not sensitive to errors in the spacecraft trajectory. However, the satellite is close enough that the uncertainty in the spacecraft position could introduce a noticeable uncertainty in the apparent position of the satellite in the sky and hence an uncertainty in the derived orbit. Based on spot checks in which orbits were fitted using slightly different trajectories, we conclude that the results presented in this paper do not suffer significantly from that effect and should be reproducible using the reconstructed trajectories available from the Navigation and Ancillary Information Facility (NAIF) at the Jet Propulsion Laboratory (JPL).[1]

2.3. *Satellite Image Measurements*

The measurement of point-source positions was discussed above; resolved sources were measured by finding the centroid.

[1] See http://naif.jpl.nasa.gov.

TABLE 2
SUMMARY OF *Cassini* OBSERVATIONS

Body	No. Obs.	Start	End
Atlas	213	2004 May 26 06:51:10.00	2005 Oct 19 11:00:09.00
Pan	77	2004 May 26 01:11:05.00	2005 Aug 31 08:17:14.00
Prometheus	1038	2004 Feb 9 22:42:24.00	2005 Nov 6 23:37:06.00
Pandora	1163	2004 Feb 12 13:39:05.00	2005 Oct 29 11:43:19.00
Janus	1376	2004 Feb 6 03:12:06.00	2005 Nov 4 19:58:54.00
Epimetheus	1360	2004 Feb 6 03:12:06.00	2005 Nov 5 07:25:09.00
Methone (S/2004 S1)	107	2004 May 12 01:12:25.00	2005 Oct 1 12:51:09.00
Pallene (S/2004 S2)	80	2004 Apr 18 04:31:24.00	2005 Nov 1 07:22:05.00
Polydeuces (S/2004 S5)	125	2004 Apr 2 05:42:24.00	2005 Oct 5 18:46:38.00
Daphnis (S/2005 S1)	38	2005 Apr 13 07:00:29.00	2005 May 1 10:11:30.00

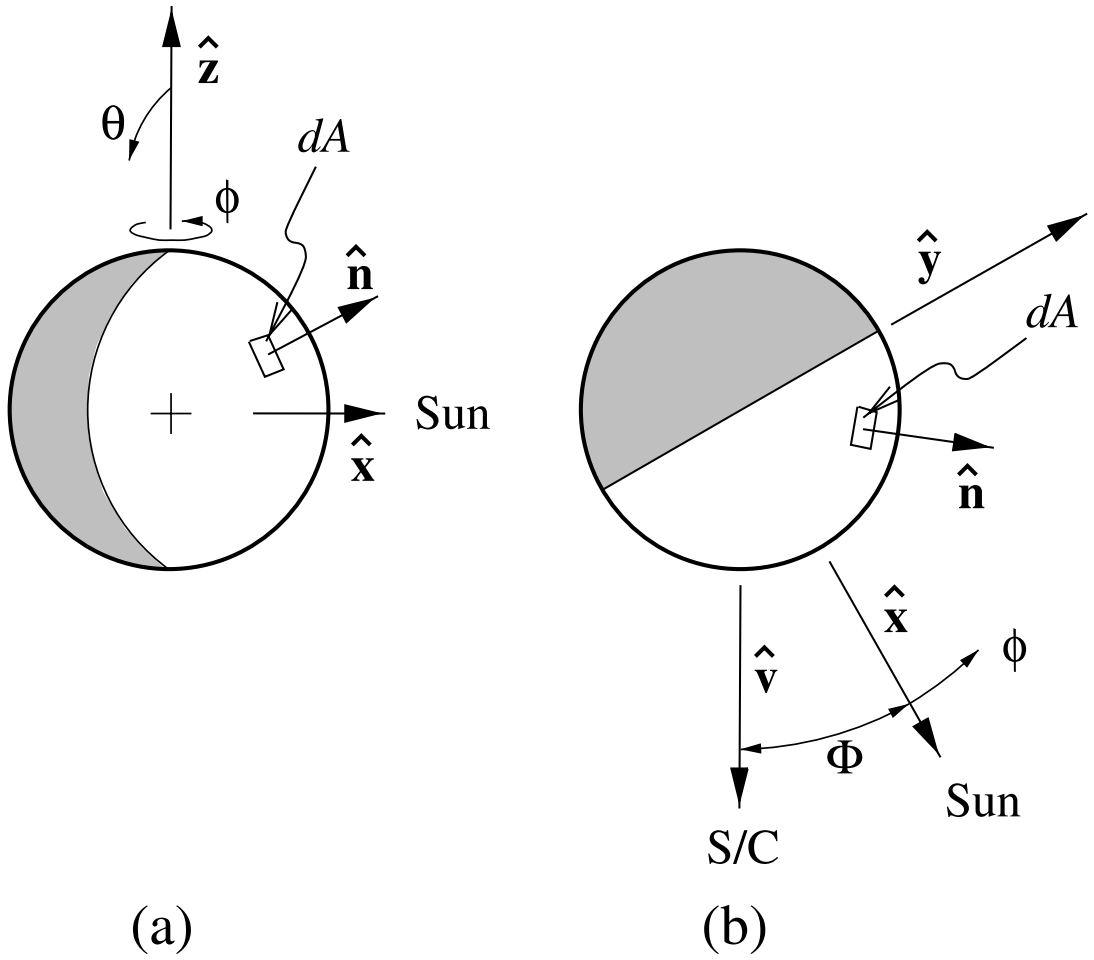

FIG. 1.—Geometry for computing phase contributions from an unresolved spherical body. Here $\hat{\boldsymbol{x}}$ points at the Sun, $\hat{\boldsymbol{z}}$ is perpendicular to $\hat{\boldsymbol{x}}$ and in the sky plane, and $\hat{\boldsymbol{y}}$ is perpendicular to $\hat{\boldsymbol{x}}$ and in the phase plane, forming a right-handed orthogonal coordinate system. Also, θ and ϕ are the standard polar coordinate angles, dA is an element of surface area with $\hat{\boldsymbol{n}}$ the surface normal at that point, Φ is the phase angle, and $\hat{\boldsymbol{v}}$ points at the observer. In (*a*), the body is shown as viewed by the observer. Panel *b* shows the body from above the $\hat{\boldsymbol{z}}$-axis.

In either case, the raw measurement gives the line and sample of the center of light in the image, which may not correspond with the center of the disk. Therefore, a phase correction was applied. Referring to Figure 1, for a spherical body with a lunar-like photometric function (i.e., no limb darkening) the offset of the center of light from the center of the disk is given by

$$c = \frac{\int_0^{\pi}\int_{-\pi/2}^{\pi/2-\Phi} R\sin(\phi+\Phi)[\hat{\boldsymbol{n}}(\theta,\phi)\cdot\hat{\boldsymbol{v}}]\,dA}{\int_0^{\pi}\int_{-\pi/2}^{\pi/2-\Phi}[\hat{\boldsymbol{n}}(\theta,\phi)\cdot\hat{\boldsymbol{v}}]\,dA} = \frac{4R}{3\pi}\frac{\sin^2\Phi}{1-\cos\Phi}, \quad (1)$$

where dA is the element of surface area, $R^2\sin\theta\,d\theta\,d\phi$, R is the apparent radius of the object in pixels, Φ is the phase angle, $\hat{\boldsymbol{n}}$ is the surface normal at spherical coordinate (θ, ϕ), and $\hat{\boldsymbol{v}}$ is the vector from the body center to the observer. The dot product ($\hat{\boldsymbol{n}}\cdot\hat{\boldsymbol{v}}$) foreshortens the surface element relative to the observer, and $R\sin(\phi+\Phi)$ is the moment of the surface element projected onto the axis in the phase plane perpendicular to the viewing direction. The moment along the $\hat{\boldsymbol{z}}$-axis is zero by symmetry. Although the assumptions leading to equation (1) are not precise, it produces a more accurate estimate of the true subpixel image position of the body center than the raw center-of-light measurement.

The raw image measurements and pointing angles (i.e., Euler angles describing the celestial orientation of the camera) for all of the *Cassini* ISS observations are tabulated in Table 3. Data from *HST* and the Earth-based stations are published elsewhere (Table 1), and the *Voyager* measurements will be published soon.

Celestial coordinates (i.e., directions corresponding to measured image locations) were determined using the instantaneous spacecraft position and orientation (from SPICE files [Acton 1996], available from the NAIF Web site) and the known geometry of the ISS cameras relative to the spacecraft (the basic geometry is described in Porco et al. [2004], and the most current information is maintained in SPICE files).

3. ORBIT MODELS

Two different approaches were used to determine orbits, depending on whether or not the body was expected to be significantly influenced by the perturbations of other satellites and how long a time was spanned by the observations.

When the body's orbit over the observation time interval was expected to be free of measurable perturbations from other satellites, the orbit was modeled as an inclined Keplerian ellipse whose apse and node precess under the influence of Saturn's gravitational harmonics. When the body's orbit was found not to be well fitted by such a simple model, numerical orbital integrations (including the effects of other satellites) were performed instead. Our work has shown that Methone, Pallene, Polydeuces, Prometheus, Pandora, Janus, Epimetheus, and even Atlas require

TABLE 3
SATURNIAN SATELLITE IMAGE MEASUREMENTS

Image	Mid-Time (UTC)	R.A.[a]	Decl.[a]	Twist[a,b]	Line[c]	Sample[c]
			Pan			
N1455932046[d]	2004 Feb 20 01:11:05.00	35.8992	9.8730	177.8793	714.59	531.47
N1455937507[d]	2004 Feb 20 02:42:06.00	35.8576	9.9471	177.8738	926.49	255.88
N1458349882[d]	2004 Mar 19 00:48:05.00	36.3377	9.8904	177.8895	200.03	571.64
N1459591410[d]	2004 Apr 2 09:40:05.00	36.4837	9.8688	177.9427	12.47	644.91
N1460506536[d]	2004 Apr 12 23:52:05.00	35.9867	9.9141	177.8949	857.99	333.47
N1462660850[d]	2004 May 7 22:17:05.00	36.8478	9.8541	177.9839	293.75	519.87
N1463416135[d]	2004 May 16 16:05:05.00	37.0183	9.9910	198.4646	56.29	591.24
N1463514356[d]	2004 May 17 19:22:06.00	37.0162	10.0873	198.4320	127.88	245.31
N1463932919[d]	2004 May 22 15:38:06.00	36.2751	9.8343	198.5387	992.77	462.99
N1464292411[d]	2004 May 26 19:29:35.00	36.4122	9.9022	178.1759	762.00	543.00

NOTE.—Table 3 is published in its entirety in the electronic edition of the *Astronomical Journal*. A portion is shown here for guidance regarding its form and content.

[a] Pointing angles are in degrees and are referenced to Earth's mean equator at the J2000.0 epoch.

[b] Twist is the angle, measured clockwise about the optic axis, between the spacecraft $\boldsymbol{X}$ vector (Porco et al. 2004) and the projection of the celestial north vector on the focal plane.

[c] Line and sample start at (1, 1) at the center of the first pixel in the image file.

[d] Provided by the JPL navigation team.

the latter approach to produce convergent and reasonable results. F-ring objects may also require such integrations. For Pan and the Keeler gap satellite, we used the Keplerian ellipse model, which we describe in the following section.

4. KEPLERIAN ELLIPSE ORBIT SOLUTIONS

The position of a body following a uniformly precessing Keplerian elliptical orbit is specified by nine elements: semimajor axis a, eccentricity e, inclination i, longitude of periapse ϖ, longitude of ascending node Ω, mean longitude at epoch λ, mean motion $n = \dot{\lambda}$, apsidal precession rate $\dot{\varpi}$, and nodal precession rate $\dot{\Omega}$.

Each Saturn-centered Keplerian elliptical, inclined solution is referred to the Saturn equator, with apse and node that precess under the influence of Saturn's gravitational harmonics. For the current orbits we took the orientation of Saturn's pole and the values of the harmonics from Jacobson et al. (2005). Because the eccentricities and inclinations of all objects are small, we use the equinoctial (Broucke & Cefola 1972) rather than the classical Keplerian orbital elements to represent the orbits:

$$
\begin{aligned}
a &= \text{geometric semimajor axis},\\
h &= e\sin\varpi,\\
k &= e\cos\varpi,\\
\lambda &= M + \varpi = M + \omega + \Omega,\\
p &= \tan(i/2)\sin\Omega,\\
q &= \tan(i/2)\cos\Omega,
\end{aligned}
$$

where e is the eccentricity, M is the mean anomaly, ω is the argument of periapse, i is the inclination to Saturn's equator, Ω is the longitude of the ascending node on Saturn's equator, λ is the mean longitude, and ϖ is the longitude of periapse. Longitudes are measured from the ascending node of Saturn's equator on that of the Earth's equator at the J2000.0 epoch in the prograde direction. The three longitude rates associated with the elements are $d\lambda/dt$, $d\varpi/dt$, and $d\Omega/dt$.

The elements were optimized using a Levenberg-Marquardt algorithm (Press et al. 1992), whereby the parameter shifts at each step are computed from the gradient and curvature of the χ^2 function. The χ^2 function is computed from the differences between the measured image locations and those computed using the instantaneous orbit solution.

Table 4 gives the orbital solutions with their formal uncertainties for the Kepler-model orbits, and Figure 2 shows the distribution of the observations in true anomaly. The element uncertainties were computed from the curvature of the χ^2 function with respect to each element (i.e., the square root of the diagonal elements of the covariance matrix [Press et al. 1992]) using an input uncertainty estimate of ± 1 pixel in line and sample. This estimate allows for not only the direct error in the measurement of the line and sample of the point source (which is in almost all cases smaller than 1 pixel) but also the indirect errors resulting from uncertainties in the pointing and in the trajectory, which are manifested as a line and sample offset in the computed position of the body at each step. In some cases, notably for the node and periapse longitudes, the effective uncertainty may be considerably larger than the quoted formal uncertainty due to various conditions such as low inclinations or eccentricities and strong correlations with other free parameters.

4.1. *Pan*

The presence of Pan in the Encke gap was first inferred by its effect on the gap's edges as seen in *Voyager* images (Cuzzi &

TABLE 4
SATURN EQUATORIAL PLANETOCENTRIC ELEMENTS FOR PAN AND DAPHNIS

Element	Pan	Daphnis
Epoch (JED)	2451545.0	2453491.9
a (km)[a]	133584.0(1)	136504.98(2)
e	0.0000348(72)	0
i (deg)	0.0010(6)	0
λ (deg)	146.588(8)	222.952(2)
ϖ (deg)	176(13)	0
Ω (deg)	20(34)	0
n (deg day^{-1})	626.031737(4)	605.9790(1)
$\dot{\varpi}$ (deg day^{-1})	3.20685(6)	0
$\dot{\Omega}$ (deg day^{-1})	−3.19059(6)	0

[a] Semimajor axis of the ellipse; independent of n.

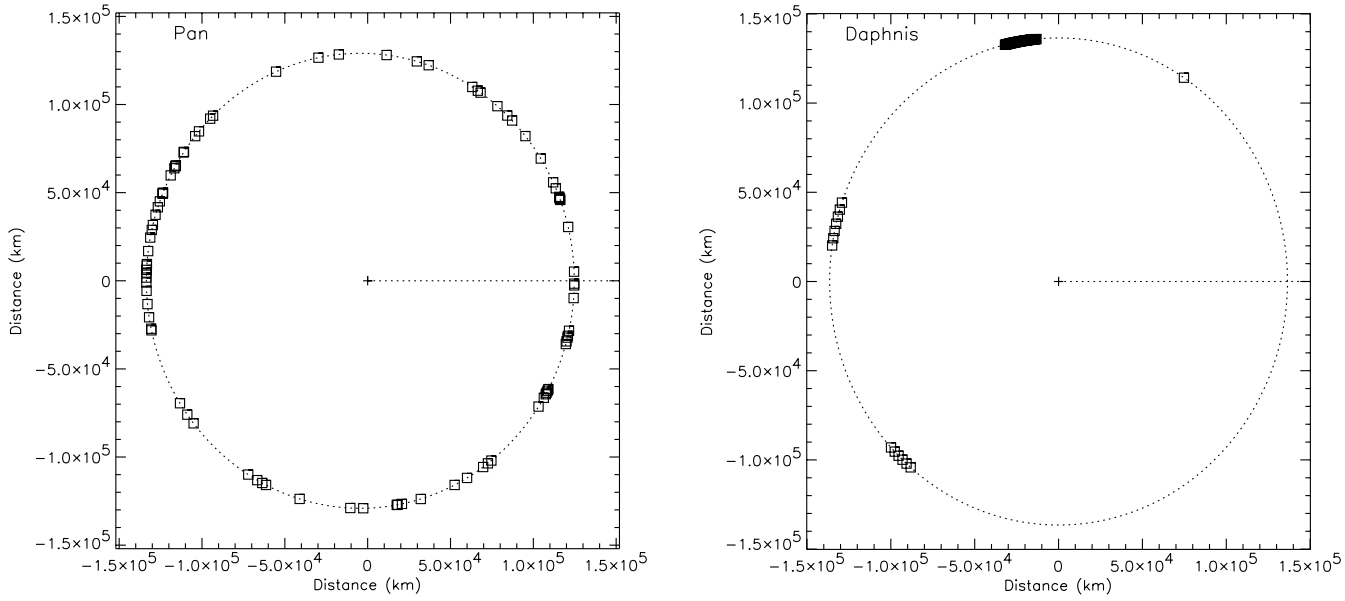

FIG. 2.—Polar plots of radius vs. true anomaly for the Pan and Daphnis observations. Periapse is to the right, with true anomaly increasing counterclockwise. The scale is in kilometers.

Scargle 1985); it was eventually observed by Showalter (1991). It has never been seen from the Earth, but it was recovered in *Cassini* images obtained on 2004 May 26.

To determine Pan's orbit, we fitted the precessing ellipse to the 23 original *Voyager 2* observations and 77 *Cassini* observations, which were made between 2004 May 26 and 2005 August 31 (see Table 3). We have extended the baseline of *Cassini* Pan observations by about 14 months over that reported in Porco et al. (2005). Showalter (1991) determined the camera pointing from the location of the Encke gap and other image features, e.g., the shadow boundary on the rings, Saturn's limb and terminator, and the outer edge of the B ring.

When processing the *Voyager* data, we accounted for the trajectory errors by estimating corrections to the approach asymptote direction (Jacobson 1991). We found the corrections in right ascension and declination to be $0\overset{\circ}{.}0285 \pm 0\overset{\circ}{.}0064$ and $0\overset{\circ}{.}0029 \pm 0\overset{\circ}{.}0018$, respectively.

Pan's classical elements, derived from the equinoctial, appear together with their formal errors in Table 4. We did not estimate a, $d\varpi/dt$, or $d\Omega/dt$ but instead computed their values from the secular perturbation formulae given in Null et al. (1981); their uncertainties are based on the errors in the mean motion and in the second zonal harmonic of Saturn's gravity field.

The addition of the *Cassini* data has improved knowledge of the mean longitude rate of Pan by 3 orders of magnitude over Showalter's published value. The Showalter (1991) orbit was circular and in Saturn's equatorial plane; we detect no significant inclination and, contrary to what we found in Porco et al. (2005), we obtain only a small eccentricity using the longer data arc. We tried an integration to check for a long-timescale variation and found very little difference from the Keplerian fit. The larger eccentricity reported in Porco et al. (2005) may have been caused by systematic errors in the *Voyager* data, which had a higher weight in that fit because there was less *Cassini* data available at the time. The integration did reveal the effect of a nearby 16:15 inner mean longitude resonance with Prometheus with a libration period of about 108 days and an amplitude of about 3 km in the in-orbit direction. The argument for that libration is

$$\theta = 16\lambda' - 15\lambda - \varpi', \tag{2}$$

where the unprimed quantities refer to Pan and the primed quantities refer to Prometheus.

Table 5 gives the postfit rms of the observation residuals. Note that the *Voyager* observations are defined in terms of right ascension (α) and declination (δ) as seen from the spacecraft, whereas the *Cassini* observations are the actual sample and line locations of Pan's image.

4.2. *Keeler Gap Satellite, Daphnis*

Porco et al. (2005) noted "wispy" features in high-resolution day-side images of the Keeler gap acquired immediately after the *Cassini* orbit insertion maneuver in 2004 July. Although their morphology remains unexplained, a frequency analysis of those features suggested that they might be associated with a satellite orbiting near the center of the gap. Such a satellite, provisionally named Daphnis, was indeed discovered in a sequence of images taken on 2005 May 1 (Porco 2005), which was part of a

TABLE 5
FIT STATISTICS FOR PAN AND DAPHNIS

	Voyager 2			*Cassini*		
OBJECT	No.	α rms (arcsec)	δ rms (arcsec)	No.	Sample rms	Line rms
Pan	23	8.30	1.45	77	0.279	0.363
Daphnis	...	...	...	38	0.977	0.923

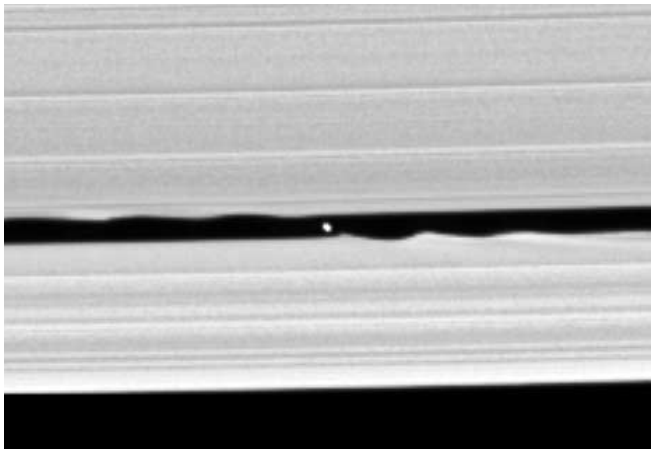

FIG. 3.—Daphnis (S/2005 S1), the Keeler gap satellite, seen on 2005 May 5. This image is from the *Cassini* Imaging Team and NASA JPL SSI.

movie designed to search for gap-embedded moonlets. Figure 3 shows a representative image from that sequence. Daphnis's disk was barely resolved, and its diameter is inferred to be about 7 km.

Daphnis's orbit was determined by fitting the precessing Keplerian ellipse model to 38 observations of line and sample, taken over about 7 months (see Table 3). The best-fit elements are given in Table 4 and the fit statistics appear in Table 5.

5. ORBITAL INTEGRATIONS

Because simple Keplerian ellipse models were inadequate to explain the motions of Methone, Pallene, Polydeuces, Atlas, Janus, Epimetheus, and of course Prometheus and Pandora (which are known to exhibit chaotic motion [Goldreich & Rappaport 2003; Renner et al. 2005]), the model for their orbits is a numerical integration of their equations of motion.

The general formulation is in Cartesian coordinates centered at the Saturnian system barycenter and referenced to the International Celestial Reference Frame. We include the perturbations on them due to the Sun and Jupiter, the asphericity of Saturn, and the major Saturnian satellites—Mimas, Enceladus, Tethys, Dione, Rhea, Titan, Hyperion, and Iapetus. Only for the cases of Atlas, Prometheus, Pandora, Janus, and Epimetheus do we also include the gravitational interactions among those five bodies. The Saturnian system dynamical parameters and the ephemerides of the perturbing satellites are from Jacobson et al. (2005). JPL planetary ephemeris DE410 (Standish 2003) provides the positions of the Sun and Jupiter.

5.1. *Methone and Pallene*

Methone (S/2004 S1) and Pallene (S/2004 S2) were discovered in *Cassini* images from 2004 June 1 between the orbits of Mimas and Enceladus on orbits that are nearly circular and uninclined (Porco 2004a; Porco et al. 2005; see Table 3 and Figure 4 for observational details). Both bodies were subsequently detected in other imaging sequences, including several "retargetable" observations designed specifically for the purpose of recovering those bodies.

With the discovery of Methone and Pallene the possibility arose that one of these satellites might be the same as an object, S/1981 S14, seen in a single *Voyager 2* image (Porco et al. 2005). The image in question was shuttered on 1981 August 23 and contained a streak that was identified as possibly being a previously unknown Saturnian satellite and given the designation S/1981 S14 (Synnott 1986). The orientation of that streak was consistent with an object on a regular orbit about Saturn, and Synnott (1986) estimated a radial distance of about 2.1×10^5 km, assuming the body was in the equatorial plane. That rough estimate would put it on an orbit very similar to that of Pallene (see Table 6). However, S/1981 S14 was revisited by Gordon et al. (1996), who concluded that the radial distance was actually about 21,000 km smaller, the discrepancy being caused by "poor camera pointing." That estimate would give S/1981 S14 an orbit similar to that of Methone. We have revisited S14 yet again and conclude, based on our own pointing, that its radial distance on an uninclined orbit would indeed be about 2.1×10^5 km, identical to Synnott's original estimate, making it a candidate for the original discovery of Pallene.

The source of the above disagreement (which amounts to >200 Vgr NAC pixels) between our estimate and that of Gordon et al. (1996) is not clear. Our pointing is derived from the position of the single bright star in the image, as was the Gordon et al. (1996) pointing. Synnott (1986) does not describe his pointing correction, but he was aware of the bright star in the center of the image, as he pointed it out in Figure 4*c* of that work. Because only one star was used for the pointing, the twist angle about the optic axis could not be constrained. However, even if the angular errors in the *Voyager* pointing were as large as an entire narrow-angle frame (about $\frac{1}{3}^\circ$, which is large even for *Voyager*), the answer would be changed by no more than a couple of pixels. Our computed longitude for S14 is within 2° of that determined by Gordon et al. (1996); since that longitude is measured in the rotating frame, that error may be caused by the use of a slightly different planetary rotation rate, which would of course not affect the radial result. Neither Synnott (1986) nor Gordon et al. (1996) provide their pole directions, but the dispersion in reasonable pole directions alone is not large enough to cause the discrepancy in radius. Parallax caused by the $\sim$10 km uncertainty in *Voyager 2*'s trajectory or Saturn's position and distortions in the image caused by the *Voyager* Vidicon system also do not account for the difference.

In spite of the unexplained radial discrepancy, 1981 S14's longitude is consistent with the predicted position of Pallene at the 1981 S14 epoch to within the roughly 8° uncertainty in Pallene's longitude (based on the mean motion in Table 6). Also, inclusion of the *Voyager* 1981 S14 measurement, together with the *Cassini* measurements, in the Pallene uniformly precessing model produces an orbit solution with an rms residual of about 2 pixels, slightly higher than without the *Voyager* measurement. However, in an *orbital integration* of Pallene's motion the S14 point exhibits a residual of about 0.6 pixels. Therefore, we conclude that S/1981 S14 and Pallene are the same object and adopt the solution given in Table 6.

Precessing ellipse models were found to be inadequate not only for the orbit of Pallene but for that of Methone as well. The orbits of both bodies have been integrated together, although their mutual perturbations were ignored because of their exceedingly small size and large distance from one other. The orbit integration clearly shows that Methone experiences significant perturbations from Mimas, and Pallene from Enceladus.

We developed a set of mean orbital elements for each satellite by fitting a precessing ellipse to the integration results over the time span 2004 January 1 to 2020 January 1. The fit included 107 *Cassini* images of Methone and 80 of Pallene (Table 3). We also included the *Voyager 2* observation of Pallene. The first Methone image in our analysis was acquired on 2004 May 12 and the last on 2005 October 1. The *Cassini* data arc for Pallene began on 2004 April 18 and ended on 2005 November 1. The resulting elements are presented in Table 6, and the statistics of

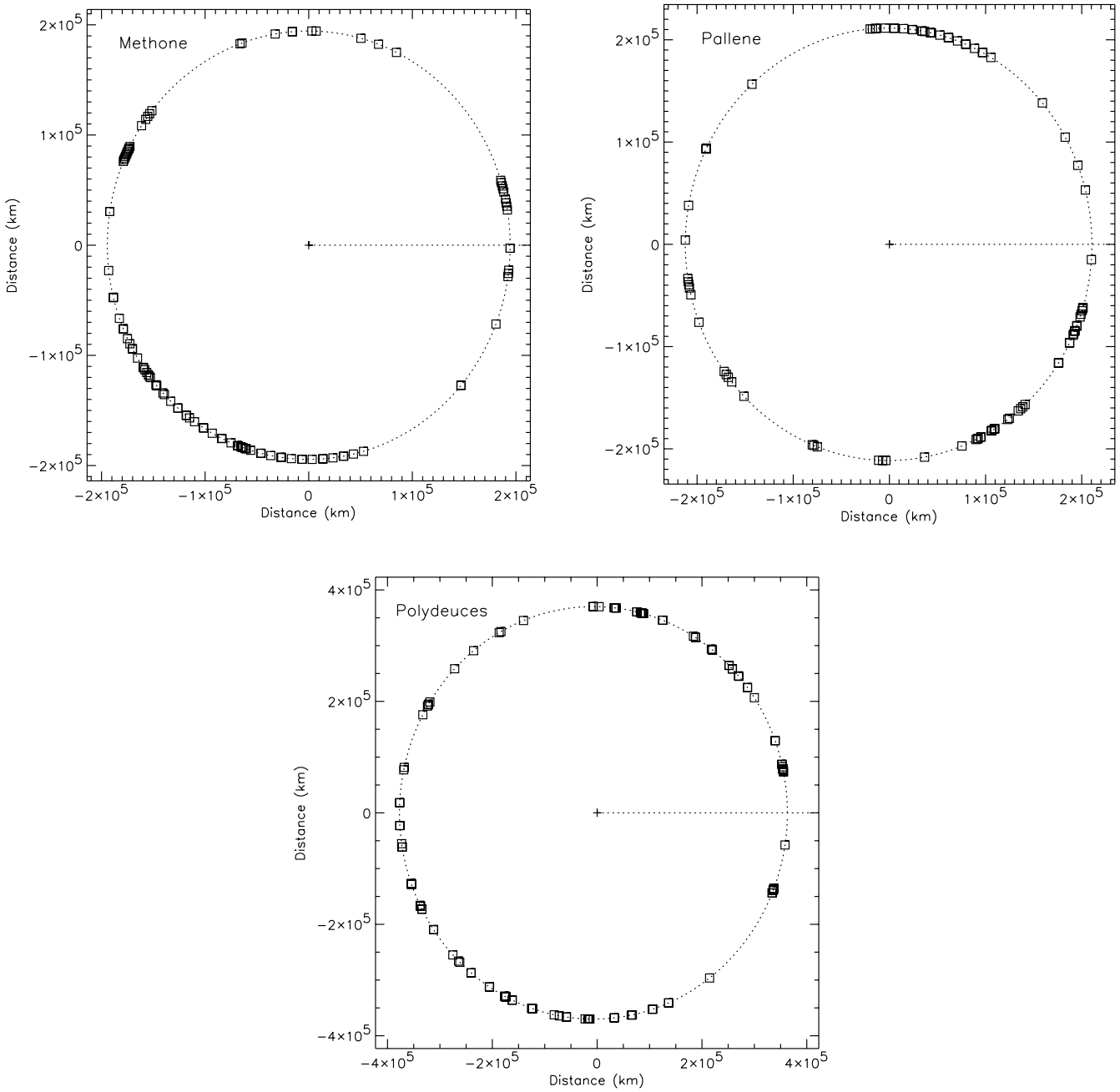

FIG. 4.—Polar plots of radius vs. true anomaly for the observations of the newly discovered satellites Methone, Pallene, and Polydeuces. Periapse is to the right, with true anomaly increasing counterclockwise. The scale is in kilometers.

TABLE 6

SATURN EQUATORIAL PLANETOCENTRIC ELEMENTS FOR METHONE, PALLENE, AND POLYDEUCES FITTED TO THE INTEGRATION OVER THE TIME SPAN FROM 2004 JANUARY 1 TO 2009 JANUARY 1

Element	Methone	Pallene	Polydeuces
Epoch (JED)	2453177.5	2453177.5	2453006.5
a (km)[a]	194440.0	212280.0	377200.
e	0.0001	0.0040	0.0192
i (deg)	0.0072	0.1810	0.1774
λ (deg)	190.9750	125.4814	107.5819
ϖ (deg)	140.9562	78.2780	144.9124
Ω (deg)	149.9364	7.2739	304.7164
n (deg day^{-1})	356.5860539	312.0271303	131.5347441
$\dot{\varpi}$ (deg day^{-1})	1.4332	0.62426	0.085095
$\dot{\Omega}$ (deg day^{-1})	−0.99889	−0.62302	−0.082562

[a] Semimajor axis of the ellipse; independent of n.

TABLE 7
FIT STATISTICS FOR METHONE, PALLENE, AND POLYDEUCES

Satellite	No.	Sample Mean	Sample σ	Sample rms	Line Mean	Line σ	Line rms
Methone	108	−0.073	0.202	0.214	−0.038	0.187	0.190
Pallene	91	−0.016	0.156	0.156	0.007	0.194	0.193
Polydeuces	129	−0.030	0.261	0.262	−0.022	0.229	0.229

the *Cassini* observation residuals are given in Table 7. The sample and line residuals for the Pallene *Voyager 2* observation on 1981 August 23 are −0.539 and +0.297, respectively.

We do not report uncertainties for elements derived by fitting a Keplerian ellipse to an orbital integration because that procedure does not produce formal uncertainties in the same sense as in the simple Keplerian fits. However, based on the formal covariance from the orbit fit and comparisons with previously determined orbits, we estimate the 1 σ error in Methone's orbit to be about 20 km in the radial direction, 400 km along the orbit, and 10 km normal to the orbital plane; the along-orbit error is basically an error in the amplitude of the mean longitude resonance with Mimas (see below). For Pallene the respective errors are 5 km radial, 20 km in orbit, and 5 km out of plane.

Figures 5 and 6 show the differences between the precessing ellipses and the integrated orbits in the directions along the orbital motion, radial from Saturn, and normal to the orbit plane. The periodic signature in the Methone in-orbit differences is a consequence of the roughly 450 day libration due to a 15:14 outer mean longitude resonance with Mimas; the resonance can be more clearly seen in Figure 7, which displays the osculating elements. The libration argument is

$$\theta = 15\lambda - 14\lambda' - \varpi, \tag{3}$$

where unprimed quantities refer to Methone and primed quantities refer to Mimas. Our analysis of the interaction between Methone and Mimas has allowed us to refine Mimas's *GM* by a factor of 6 (Jacobson et al. 2006).

The in-orbit difference for Pallene also exhibits a long-period signature, and the same signature appears in Pallene's osculating mean longitude, shown in Figure 8. The long-period effect is caused by a 19:16 inner mean longitude resonance with Enceladus. Figure 9 shows the difference between an integrated orbit and a precessing ellipse when Enceladus is omitted from the integration; the periodic in-orbit signature seen in Figure 6 is no longer present. A possible argument for the libration with Enceladus is

$$\theta = 19\lambda' - 16\lambda - \varpi - 2\Omega, \tag{4}$$

where the unprimed quantities refer to Pallene and the primed quantities refer to Enceladus. The period of the libration is about 10 yr.

5.2. *Polydeuces*

Polydeuces was discovered in images from 2004 October 21 (Porco 2004c; Porco et al. 2005; Murray et al. 2005) (see Table 3). It became clear with repeated observations that Polydeuces was a Trojan of Dione. We determined its orbit by numerical integration, taking Polydeuces to be massless, owing to its small

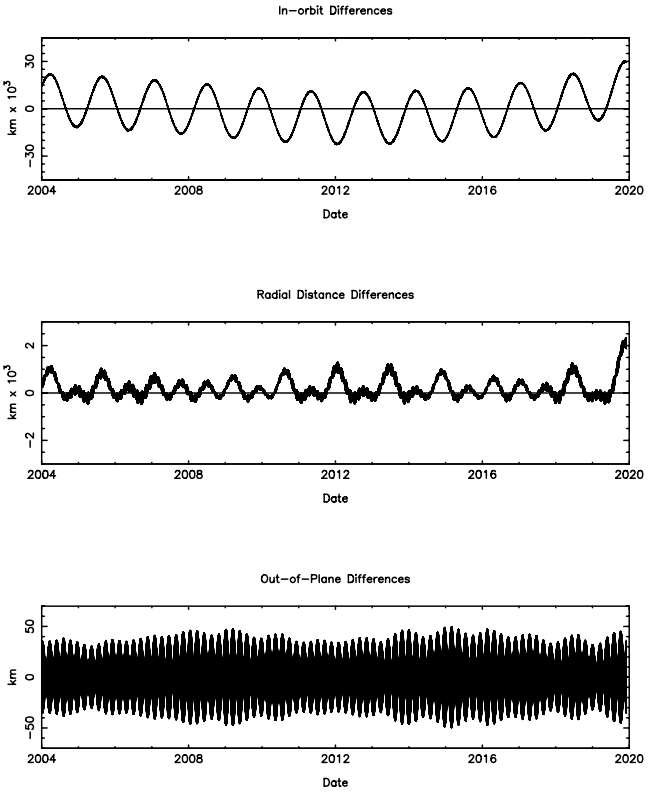

FIG. 5.—Differences between the integrated orbit and the mean precessing ellipse for Methone.

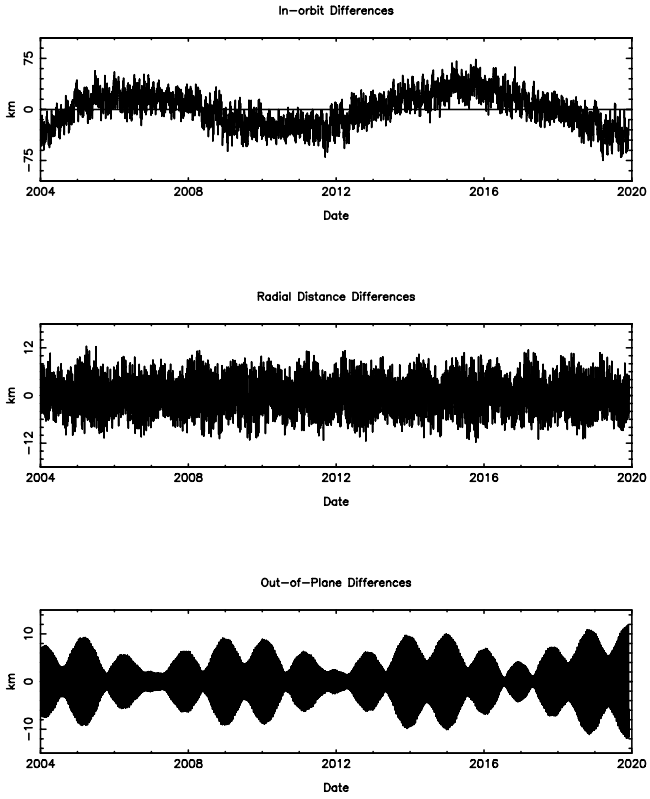

FIG. 6.—Differences between the integrated orbit and the mean precessing ellipse for Pallene.

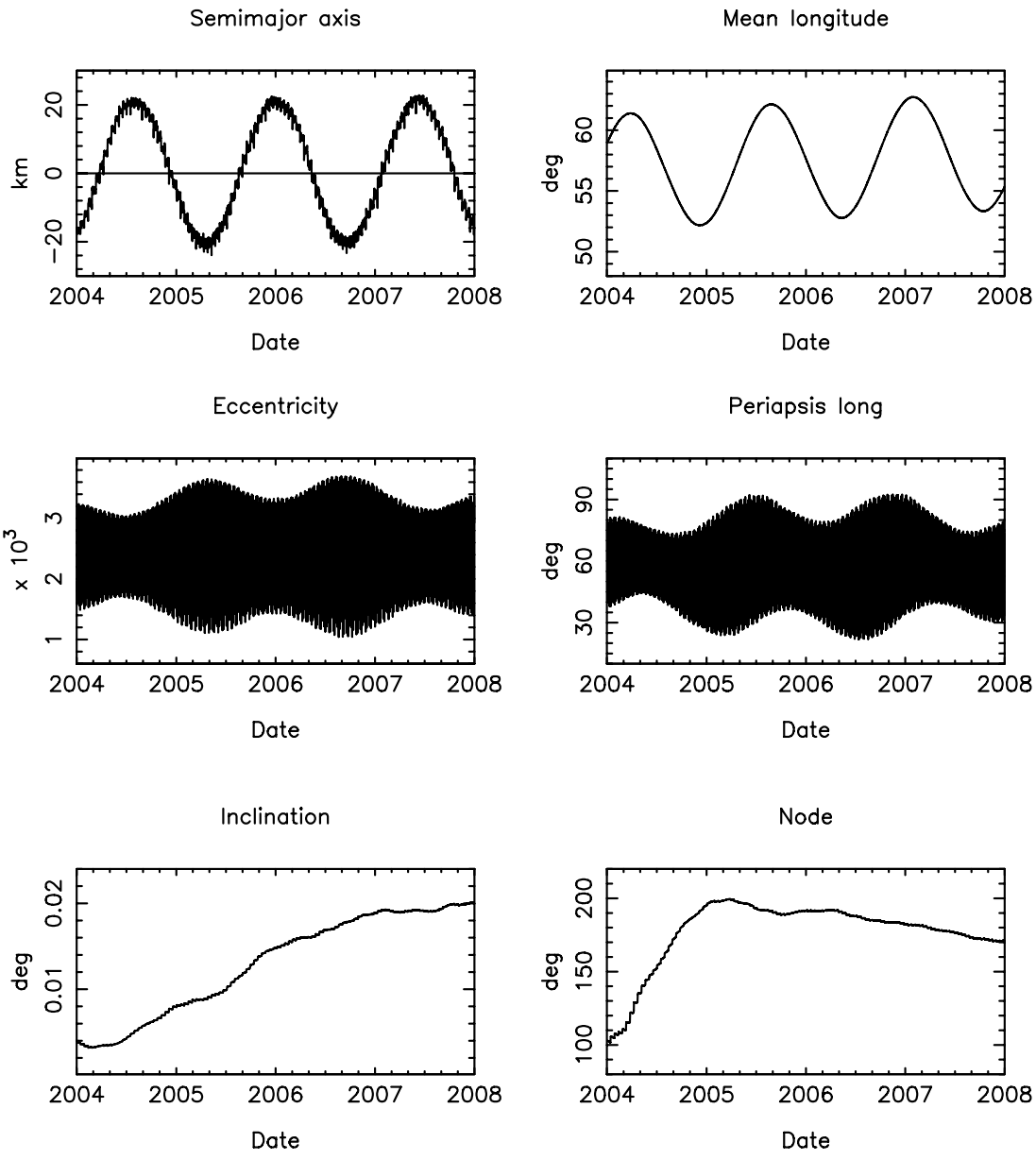

FIG. 7.—Osculating elements from the integration of Methone's orbit.

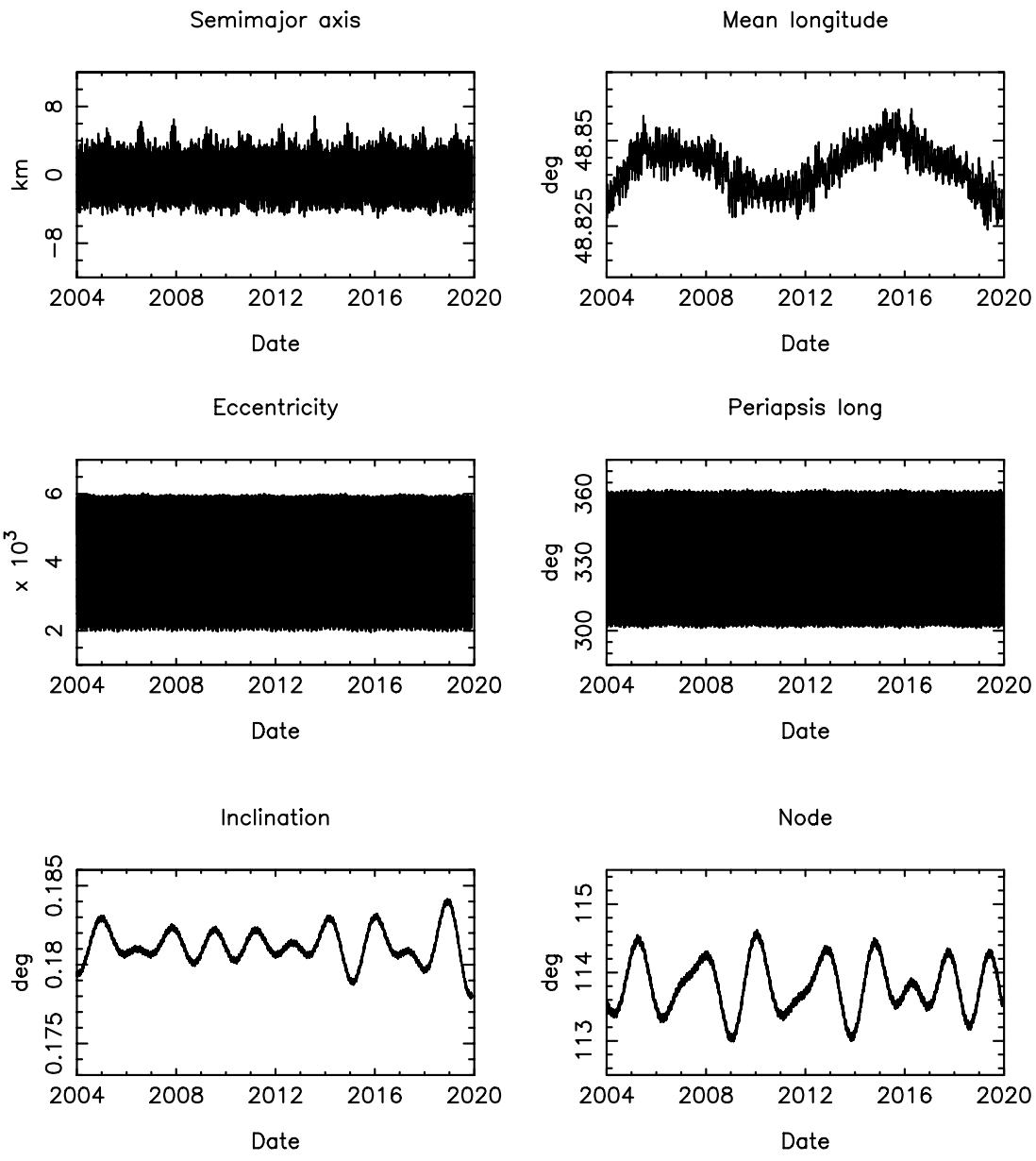

FIG. 8.—Osculating elements from the integration of Pallene's orbit.

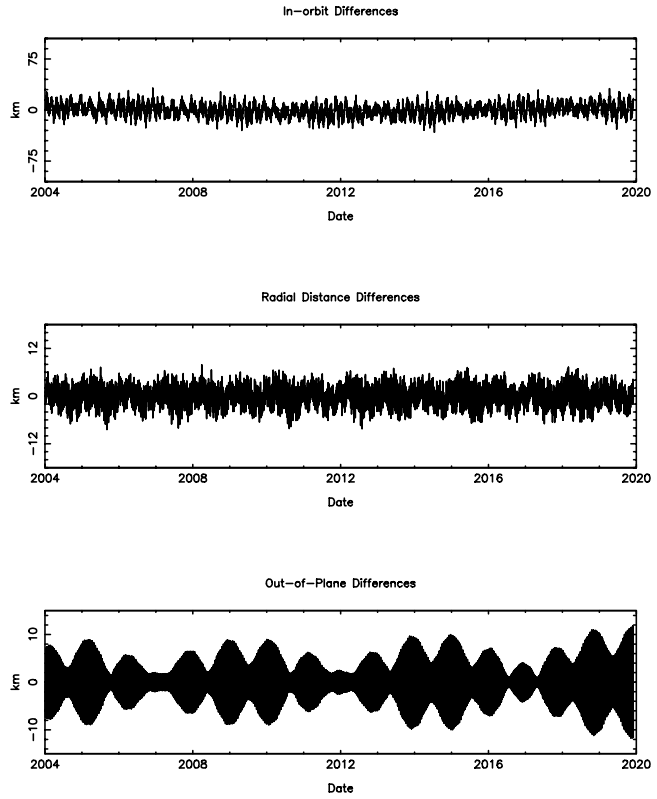

FIG. 9.—Differences between the integrated orbit and the mean precessing ellipse for Pallene with Enceladus omitted from the integration.

size. The data arc began on 2004 April 2 and ended on 2005 October 5. We find that Polydeuces is librating about Dione's trailing Lagrange point L5 (67°.87 behind Dione) with an amplitude varying between −31°.41 and +26°.06 and a period of 790.931 days (see Fig. 10). By way of comparison, Dione's previously known Lagrangian satellite, Helene, leads Dione by about 62°.46 and librates with an amplitude varying between −14°.92 and +16°.42 and a period of 767.94 days (Jacobson et al. 2005).

Our result is close to that of Porco et al. (2005), where we reported an amplitude of about ±25°.8 and a period of about 792 days. The discrepancy is caused primarily by the fact that the current fit is based on a significantly longer data arc (17.5 vs. 10 months). An independent fit by Murray et al. (2005) used a similar data set to that of Porco et al. (2005) and reported an amplitude that varied between −31°.68 ± 0°.06 and +21°.16 ± 0°.1 with a period of 791.3 days

Based on the formal covariance from the orbit fit and comparisons with previously determined orbits, we estimate the 1 σ error in the orbit to be about 5 km in the radial direction, 25 km along the orbit, and 10 km normal to the orbital plane. The error in the orbital period is less than 0.05 s.

We developed a set of mean orbital elements for Polydeuces by fitting a precessing ellipse to the integration over the time span 2004 January 1 to 2009 January 1. In the fit we corrected the mean longitude to account for the libration. Table 6 contains the derived elements. The statistics of the observation residuals are given in Table 7.

5.3. *Atlas, Prometheus, Pandora, Janus, and Epimetheus*

The refinement of Mimas's *GM* resulting from our analysis of Methone's orbit has allowed us to compute the orbits of Atlas, Prometheus, Pandora, Janus, and Epimetheus in a single integration by fitting to all of the observations and adjusting the

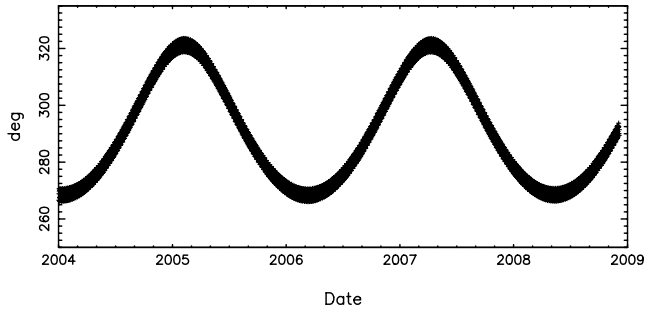

FIG. 10.—Polydeuces's orbital phase relative to Dione as a function of time. Polydeuces librates about Dione's trailing Lagrangian point L5 (67°.87 from Dione) with an amplitude varying between −31°.41 and +26°.06 and a period of 790.931 days.

satellites' initial states and *GM*s. In this integration the mutual gravitational interactions of these satellites were included, as well as the other effects mentioned above. The orbits were fitted to Earth-based, *HST*, *Voyager*, and *Cassini* observations. The orbital distributions for the *Cassini* image measurements appear in Figure 11, and the measurements themselves appear in Table 3; Tables 8 and 9 give the number and types of non-*Cassini* observations for each body. The observation type labels indicate Saturn-relative positions (labeled x and y) and Saturn-relative separation (labeled ρ). Table 2 provides the time spans of the *Cassini* observations. The *Voyager* observations are assumed to be accurate to 1 pixel for Janus and Epimetheus and 5 pixels for Atlas, Prometheus, and Pandora; the fit to the *Voyager* data is well within the measured accuracy. For the time frame of the *Cassini* tour the integrated orbits are presumed to be accurate to roughly 25 km for Janus and Epimetheus and 50 km for Atlas, Prometheus, and Pandora; the error is primarily in the downtrack direction, and radial and out-of-plane errors are less than 10 km.

Mean elements for the integrated orbits appear in Table 10; they are the elements of precessing ellipses fitted in a least-squares sense over the 2 yr time span from 2003 January to 2005 January, a relatively benign period in the satellite dynamics. The statistics for the fits appear in Table 11. The differences between the mean and integrated orbits are periodic and are largest in the along-orbit direction. Their amplitudes are as follows: 200 km, Janus; 750 km, Epimetheus; 600 km, Atlas; 40 km, Prometheus; and 1750 km, Pandora.

Janus and Epimetheus roughly share the same mean orbit but have close approaches every 4 yr, at which time they swap orbits (Yoder et al. 1983). Prometheus and Pandora have been found to be in chaotic orbits as a consequence of a mean-motion resonance (Goldreich & Rappaport 2003; Renner et al. 2005); they exhibit significant changes in their mean motions every 6.2 yr when their apses are antialigned. Moreover, Pandora is in a 3:2 mean-motion resonance with Mimas (McGhee 2000). We have found that Atlas is strongly perturbed by Prometheus and to a lesser extent by Pandora. Figure 12 shows the in-orbit differences between the integrated Atlas orbit and a precessing ellipse when the effects of Prometheus and Pandora are excluded. Figures 13 and 14 show the same difference when only the perturbations due to Pandora or Prometheus are excluded. A 54:53 mean longitude resonance with Prometheus introduces a periodic perturbation with an amplitude of about 600 km and a period of about 3 yr. The argument for that libration is likely to be

$$\theta = 54\lambda' - 53\lambda - \varpi', \tag{5}$$

where the unprimed quantities refer to Atlas and the primed quantities refer to Prometheus. The amplitude of the perturbation

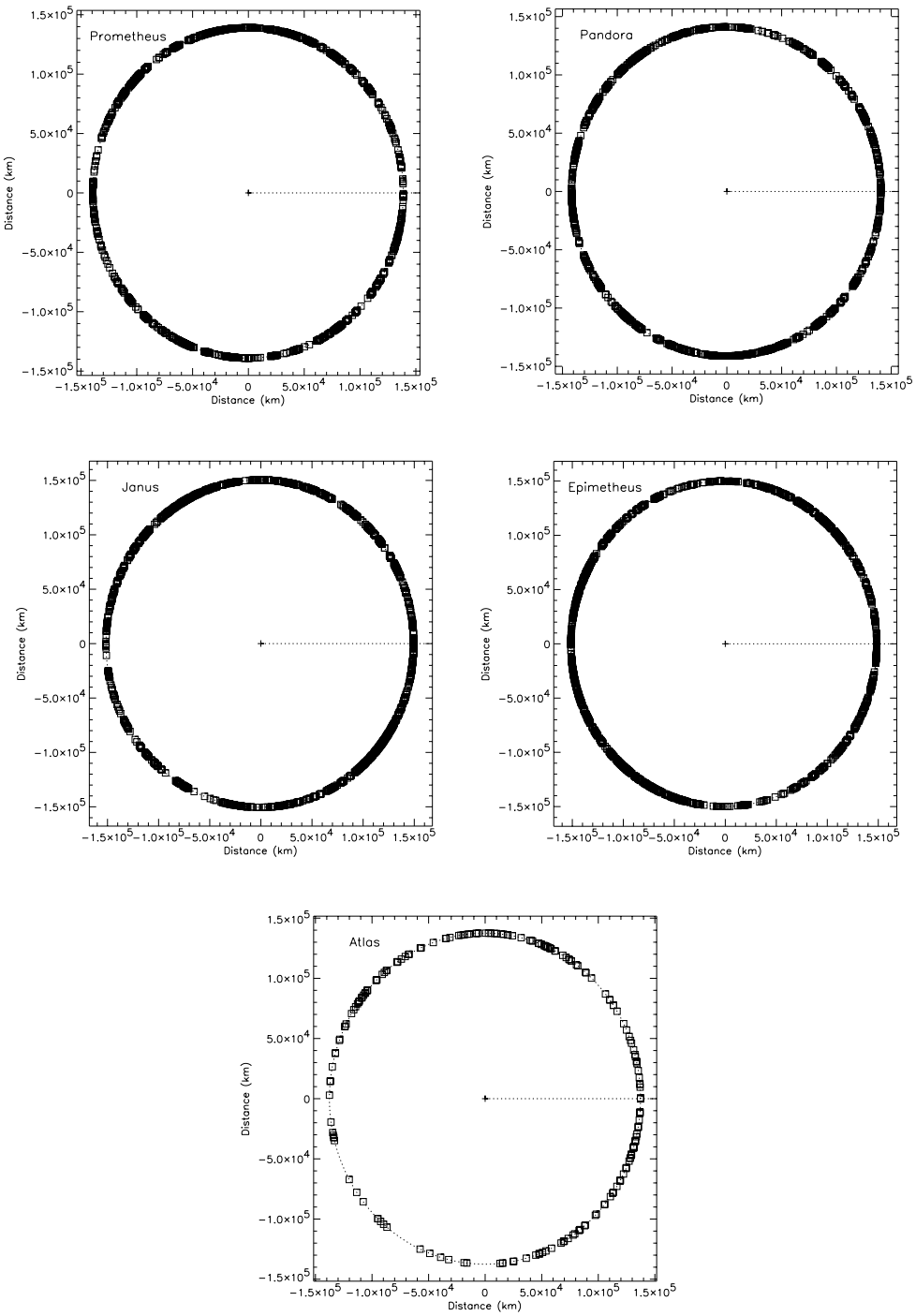

FIG. 11.—Polar plots of radius vs. true anomaly for the Prometheus, Pandora, Janus, Epimetheus, and Atlas observations. Periapse is to the right, with true anomaly increasing counterclockwise. The scale is in kilometers.

TABLE 8
HST Observation Residuals for Janus, Epimetheus, Atlas, Prometheus, and Pandora

Satellite	Type	No.	rms (arcsec)	Source
Janus	x	34	0.021	4
	y	34	0.026	4
Epimetheus	x	46	0.050	4
	y	46	0.038	4
Atlas	ρ	19	0.312	4
Prometheus	x	30	0.039	4
	y	30	0.026	4
Pandora	x	29	0.043	4
	y	29	0.025	4
Janus	x	10	0.027	1
	y	10	0.053	1
Epimetheus	x	14	0.024	1
	y	14	0.040	1
Prometheus	x	21	0.021	1
	y	21	0.037	1
Pandora	x	15	0.016	1
	y	15	0.038	1
Janus	x	180	0.011	2
	y	180	0.011	2
Epimetheus	x	171	0.011	2
	y	172	0.014	2
Prometheus	x	199	0.015	2
	y	199	0.015	2
Pandora	x	182	0.012	2
	y	182	0.013	2
Janus	x	71	0.015	3
	y	71	0.014	3
Epimetheus	x	73	0.019	3
	y	73	0.013	3
Prometheus	x	17	0.025	3
	y	17	0.021	3
Pandora	x	55	0.029	3
	y	55	0.026	3

References.—(1) R. G. French 2001, private communication (*HST* observations: 1994 December 1 to 1995 November 18); (2) French et al. 2006 (PC chip); (3) French et al. 2006 (WF chip); (4) McGhee et al. 2001.

produced by a 70:67 mean longitude resonance with Pandora is of the order of 150 km, and the period is longer than the 6.2 yr time between the Prometheus-Pandora chaotic interaction. A likely argument for that libration is

$$\theta = 70\lambda' - 67\lambda - 3\varpi', \tag{6}$$

where the unprimed quantities refer to Atlas and the primed quantities refer to Pandora. Because the "mean" motions of the bodies involved in the above resonances are dependent on the length of the integration arc, it is difficult to determine the correct combinations of the apse rates for each resonance. Therefore, we have chosen the smallest coefficients needed to produce a valid resonant argument.

The effect of the onset of the Prometheus-Pandora interaction in the year 2000 on the Atlas orbit can be seen at the end of Figures 13 and 14. As the orbits of Prometheus and Pandora are chaotic, there is reason to suspect that Atlas's orbit may be chaotic as well. If it is, then the Lyapunov timescale must be longer than the 19 month span of the *Cassini* data arc.[2]

[2] Although the total data arc for Atlas encompasses the *Voyager* missions and *HST*, the quality of those observations is poor enough that we cannot confidently rule out chaos in Atlas's orbit during the entire data arc.

The *GM*s from the fit appear in Table 12, along with several previously published values. The Janus and Epimetheus *GM*s are well determined; they have changed little from the earlier results. Our *GM*s for Prometheus and Pandora are significantly smaller than the previous results, primarily due to a rereduction and recalibration of the *HST* observations[3] and to the observed perturbations of the satellites on Atlas. Note that they are in agreement with the *GM*s found by Rosen et al. (1991) from the satellites' effects on Saturn's rings. Our Atlas *GM* is the first determination from the dynamical interaction of the satellites; Porco et al. (2005) found a *GM* of 0.00014 km^3 s^{-2} based on the effect of Atlas in raising linear density waves in Saturn's rings.

5.4. *F-Ring Objects*

The dynamical stability of objects orbiting near the F ring is likely to be complicated; their orbits are probably chaotic due to overlapping resonances from the shepherding satellites (Borderies et al. 1984), and the F ring itself may influence the orbits of nearby and embedded bodies. Moreover, if they are mere "clumps," then bodies may simply shear apart on timescales of a few months (Poulet et al. 2000; Barbara & Esposito 2002). Other interactions with Prometheus and Pandora may also assist in the destruction of F-ring objects. Therefore, with observations over a limited time span it can be difficult to determine whether or not a body seen orbiting near the F ring is actually a permanent satellite. Three objects—S/2004 S3, S4,[4] and S6—were discovered in 2004 (Porco 2004b); see Table 3. In an attempt to recover those bodies, an imaging sequence on 2004 November 15 covered about one orbital period of the F ring at a pixel scale of about 4 km, near their estimated sizes (Porco et al. 2005). For an unresolved object, the expected data value, integrated over the point spread, is roughly (Porco et al. 2004)

$$\mathrm{DN} = \frac{\alpha}{G}\frac{R^2}{D^2} t F(\Phi), \tag{7}$$

where D is the distance from the camera to the body, R is the radius of the body, t is the exposure duration, G is the gain factor (electrons DN^{-1}), and α is a calibration factor that depends on the camera and the filter combination. Here $F(\Phi)$ is a phase factor representing the fraction of the (assumed spherical) body that is seen to be lit from the viewer's perspective (refer to Fig. 1):

$$F(\Phi) = \frac{1}{\pi R^2}\int_0^{\pi}\int_{-\pi/2}^{\pi/2-\Phi} [\hat{\boldsymbol{n}}(\theta,\phi)\cdot\hat{\boldsymbol{v}}]\, dA = \tfrac{1}{2}(1+\cos\Phi). \tag{8}$$

Therefore, for two different observations of the same object using the same filter combination and the same gain state, we can define

$$\xi \equiv \frac{\mathrm{DN}_2}{\mathrm{DN}_1} = \left(\frac{D_1}{D_2}\right)^2\left(\frac{t_2}{t_1}\right)\left(\frac{1+\cos\Phi_2}{1+\cos\Phi_1}\right), \tag{9}$$

where the indices denote each observation. Values of ξ greater than or equal to $\sim$1 indicate that an object detected in observation 1 should be detectable in observation 2.

[3] Both Renner et al. (2005) and Jacobson & French (2004) used the observations from French et al. (2003) and French & McGhee (2004).

[4] S/2004 S4 was discovered in a search for additional sightings of S/2004 S3 and may be the same body. The S4 sequence occurs about 5 hr later than the S3 sequence, but the body is seen interior to the F-ring core, whereas S3 was seen *exterior* to the core.

TABLE 9

EARTH-BASED OBSERVATION RESIDUALS FOR JANUS, EPIMETHEUS, ATLAS, PROMETHEUS, AND PANDORA

Satellite	Type	No.	rms (arcsec)	Type	No.	rms (arcsec)	References
			1980 Observations				
Janus	ρ	13	0.178	...	...	...	1
Epimetheus	ρ	7	0.346	...	...	...	1
Janus	ρ	36	0.608	...	...	...	4
Janus	x	7	0.284	...	...	...	4
Epimetheus	ρ	10	0.249	...	...	...	4
Epimetheus	x	4	0.110	...	...	...	4
Pandora	ρ	4	0.223	...	...	...	4
Janus	ρ	6	0.614	...	...	...	6
Epimetheus	ρ	2	0.498	...	...	...	6
Prometheus	ρ	6	0.298	...	...	...	6
			1990 Observations				
Janus	x	8	0.126	y	8	0.156	2
Epimetheus	x	23	0.259	y	23	0.206	2
			1995 Observations				
Janus	ρ	20	0.115	...	...	...	3
Epimetheus	ρ	4	0.115	...	...	...	3
Prometheus	ρ	2	0.113	...	...	...	3
Pandora	ρ	15	0.071	...	...	...	3
			2000 Observations				
Janus	x	31	0.089	y	31	0.012	5
Prometheus	x	22	0.042	y	22	0.055	5

REFERENCES.—(1) Dollfus & Brunier 1981; (2) Nicholson et al. 1992; (3) F. Poulet & B. Sicardy 2001, private communication; (4) Seidelmann et al. 1981; (5) Sharringhausen et al. 2003; (6) Yoder et al. 1989.

TABLE 10

SATURN EQUATORIAL PLANETOCENTRIC ELEMENTS FOR JANUS, EPIMETHEUS, ATLAS, PROMETHEUS, AND PANDORA FITTED TO THE INTEGRATION OVER THE 2 YR TIME SPAN FROM 2003 JANUARY TO 2005 JANUARY

Element	Atlas	Prometheus	Pandora	Janus	Epimetheus
Epoch (JED)	2453005.5	2453005.5	2453005.5	2453005.5	2453005.5
a (km)[a]	137670	139380	141720	151460	151410
e	0.0012	0.0022	0.0042	0.0068	0.0098
i (deg)	0.003	0.008	0.050	0.163	0.351
λ (deg)	129.760	306.117	253.373	171.432	346.196
ϖ (deg)	332.021	63.893	50.676	288.678	37.847
Ω (deg)	0.500	259.504	327.215	46.899	85.244
n (deg day^{-1})	598.3099854	587.2852370	572.7885228	518.2388834	518.4828200
$\dot{\varpi}$ (deg day^{-1})	2.8781	2.7577	2.5996	2.0529	2.0553
$\dot{\Omega}$ (deg day^{-1})	−2.8678	−2.7451	−2.5879	−2.0448	−2.0473

[a] Semimajor axis of the ellipse; independent of n.

TABLE 11

IMAGING RESIDUAL STATISTICS FOR JANUS, EPIMETHEUS, ATLAS, PROMETHEUS, AND PANDORA

	VOYAGER 1			VOYAGER 2			CASSINI		
OBJECT	No.	Sample rms	Line rms	No.	Sample rms	Line rms	No.	Sample rms	Line rms
Janus	17	0.395	0.521	28	0.299	0.433	1376	0.256	0.309
Epimetheus	23	0.431	0.307	29	0.280	0.278	1360	0.322	0.331
Atlas	5	1.872	1.098	6	2.927	1.767	213	0.195	0.182
Prometheus	18	0.549	0.354	28	1.579	1.482	1038	0.257	0.241
Pandora	32	0.450	0.714	39	1.396	0.742	1163	0.272	0.287

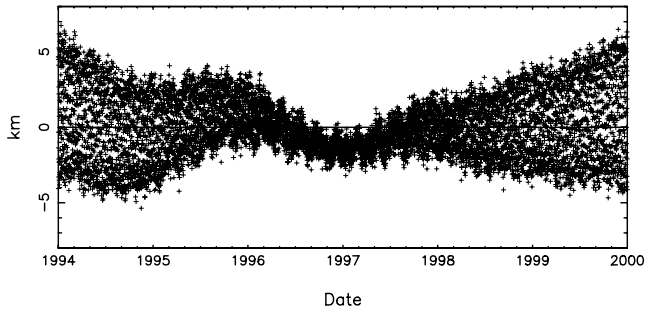

FIG. 12.—Atlas in-orbit differences, excluding Prometheus and Pandora.

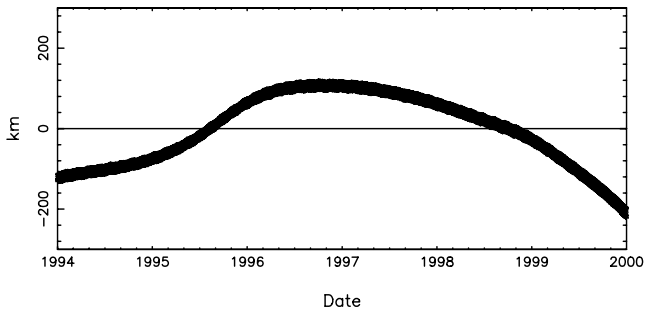

FIG. 14.—Atlas in-orbit differences, excluding only Prometheus.

The November 15 sequence was taken in the clear filters with $\Phi \sim 83^\circ$, $D \sim 4.5 \times 10^6$ km, and $t = 2$ s. The circumstances for the S3 discovery sequence were similar, but with a considerably shorter integration time, specifically, $\Phi \sim 66^\circ$, $D \sim 6.5 \times 10^6$ km, and $t = 0.68$ s, yielding $\xi \sim 4.9$. Therefore, S3 should be visible in the November 15 images. Recall that the S4 discovery sequence occurred just 5 hr later than the S3 sequence, so the circumstances for both of those discoveries were nearly identical. Moreover, that sequence was obtained through various nonclear filters, further reducing the flux at the time of discovery, so S4 should also be visible in the November 15 sequence. For S6, we had $\Phi \sim 152^\circ$, $D \sim 5.3 \times 10^5$ km, and $t = 0.05$ s in the clear filters, yielding $\xi \sim 5.3$, so S6 should be visible in the November 15 sequence as well.

Despite the preceding arguments, none of the above F-ring objects from 2004 were recovered in the November 15 sequence, suggesting that they were transient "clumps" rather than solid satellites. Alternatively, because it was only observed at high phase, S6 may have been a clump of fine material, or a small solid body buried in a halo of fine forward-scattering material, which would be difficult to detect in the relatively low phase November 15 observations, in which case those observations would have little bearing on its existence at that time. Therefore, the November 15 observations strongly suggest that S3 and S4 had disappeared by that time, and that S6 may have also disappeared unless its visibility was controlled mainly by small forward-scattering particles.

At the time of writing, at least 16 unambiguous objects—C7 through C22[5]—have been observed in orbit near the F ring in images comprising several movies (see Table 3) during 2005. In order to determine whether a given set of sightings corresponds to a single object, we search for a single orbit that fits all of the observations in question. As the individual data arcs tend to be relatively short compared to the time between sequences, a reasonable-looking orbit solution can often be found to tie together two sightings, whether or not those sightings represent the same object. In other words, each of the 2004 sightings can be tied to one or more of the 2005 sightings (S3 could be the same as C8 or C10, but so could S6), but those observations cannot all represent a single body because they are not all consistent with a single orbit, so many (probably most) of these associations are coincidental. However, as shown in Table 13, we do find that two orbits give reasonable fits to three or more sightings.

The first three-sighting solution in Table 13, with an rms residual of about 10 pixels, suggests that S/2004 S3 reappears as S/2004 S4, then C12, and finally C22 (see Fig. 15 for the true-anomaly distribution of those observations). The Keplerian fit is poor, but given the complicated dynamical environment near the F ring that might be expected. However, an orbit integration also does not converge, so either we have neglected an important perturbation (e.g., from the F ring itself) in the integration or this set of observations does not describe a single body.

The second three-sighting solution in Table 13, with an rms residual of about 9 pixels, suggests that S/2004 S6 reappears as C11, then C13, then C20, and finally C21 (see Fig. 15 for the true-anomaly distribution of those observations). Again, the simple Keplerian fit is poor, but this time the orbit integration shows promise. Figure 16 shows the osculating elements. The secular rates have been removed from the mean longitude, periapse longitude, and node. Note the jumps in semimajor axis, which indicate energy changes; there are corresponding mean-motion changes, as indicated by the kinks in the mean-longitude plot. These effects are due to the S/2004 S6 interaction with Prometheus. Figure 17 shows the differences between the integrated orbit and the precessing ellipse (mean elements). Note that the kinks in the in-orbit differences and the jumps in the radial differences match what is seen in the osculating elements. Figure 18 displays the differences between an integration that omits the Prometheus perturbation and the precessing ellipse fit to that integration. There are still kinks and jumps indicating further energy changes; these are due to Pandora. The results when Pandora is omitted from the integration appear in Figure 19. The "energy" changes are gone, but a periodic effect is now revealed. Removing Janus from the integration removes that effect, as shown in Figure 20; the remaining signatures are from the Mimas, Titan, and Epimetheus perturbations.

The above demonstrates that S/2004 S6 (assuming it is real), Prometheus, and Pandora are directly interacting and are being influenced by Janus and probably Mimas, Titan, and Epimetheus. There is much further work to be done; possibly the observations on June 21 and 29 are of S/2004 S6 and are simply indicating that we have not found all of the significant perturbations.

[5] Provisional naming of F-ring objects was approached more cautiously in 2005, now that we see how difficult it is to establish their identities. Therefore, objects discovered after 2004 are referred to in this paper using unofficial names starting with the letter "C."

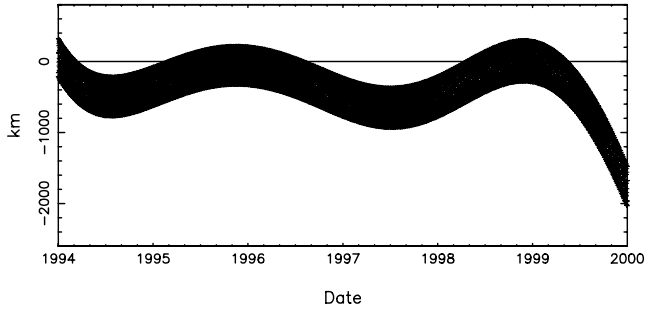

FIG. 13.—Atlas in-orbit differences, excluding only Pandora.

TABLE 12

GM Values ($km^3\ s^{-2} \times 10^{-3}$) for Janus, Epimetheus, Atlas, Prometheus, and Pandora

References	Janus	Epimetheus	Atlas	Prometheus	Pandora
7	135.5 ± 13.3	37.5 ± 3.7	...	...	...
6	87^{+113}_{-20}	28^{+11}_{-7}	...	10 ± 5	9 ± 5
3	132.1 ± 8.3	36.7 ± 2.0	...	...	...
1	128.4 ± 6.0	35.7 ± 1.7	...	...	...
5	...	...	...	$14.1^{+1.0}_{-2.5}$	$10.3^{+1.0}_{-1.9}$
2	126.9 ± 0.9	35.2 ± 0.3	...	12.0 ± 0.7	10.1 ± 0.5
4	...	...	0.14	...	...
Current work	127.58 ± 0.33	35.40 ± 0.09	0.44 ± 0.04	10.45 ± 0.13	9.05 ± 0.15

References.—(1) Jacobson 1996; (2) Jacobson & French 2004; (3) Nicholson 1992; (4) Porco et al. 2005; (5) Renner et al. 2005; (6) Rosen et al. 1991; (7) Yoder et al. 1989.

TABLE 13

Saturn Equatorial Planetocentric Elements for F-Ring Candidates with at Least Three Consistent Sightings

Element	S3/S4/C12/C22	S6/C11/C13/C20/C21
Epoch (JED)	2453474.1	2453474.1
a (km)[a]	140300(1)	140134(2)
e	0.00210(2)	0.00200(4)
i (deg)	0.0642(7)	0.002(1)
λ (deg)	185.6(8)	161.10(3)
ϖ (deg)	180.6(7)	350.1(2)
Ω (deg)	138.9(5)	142.52(2)
n (deg day^{-1})	581.86489(2)	582.5133(4)
$\dot{\varpi}$ (deg day^{-1})	2.69311(3)	2.71675(3)
$\dot{\Omega}$ (deg day^{-1})	−2.68123(3)	−2.70472(3)

[a] Semimajor axis of the ellipse; independent of n.

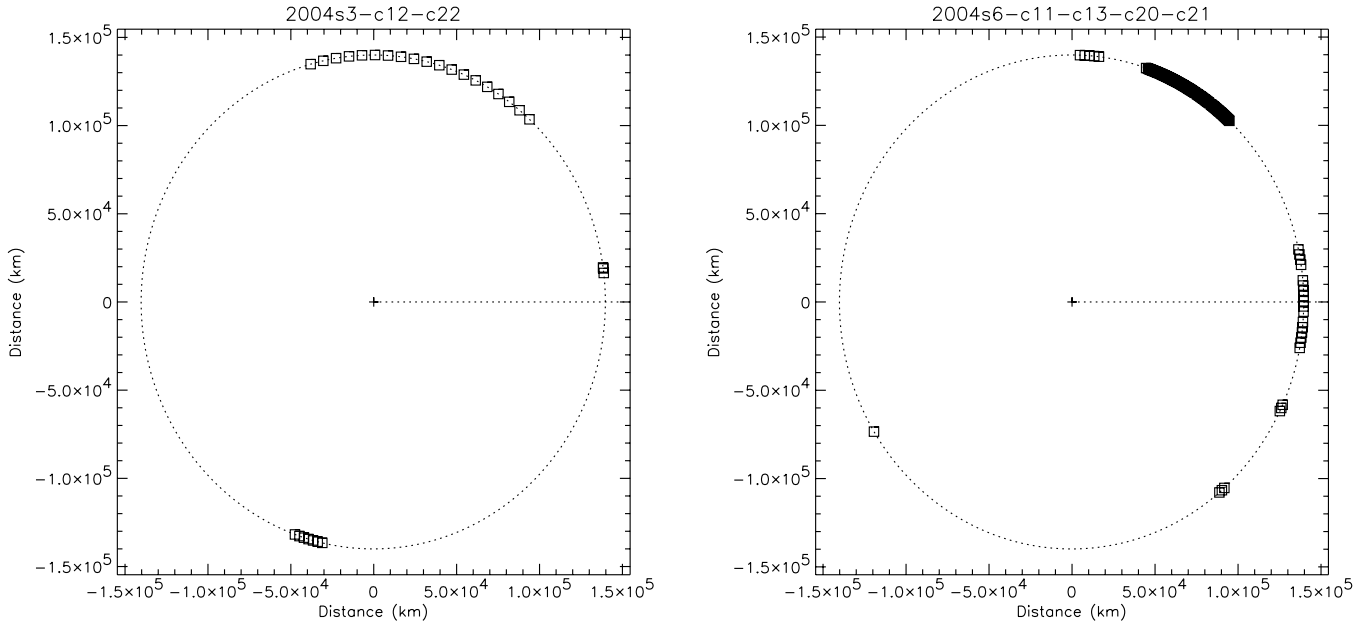

Fig. 15.—Polar plots of radius vs. true anomaly for the F-ring objects with three or more consistent sightings. Periapse is to the right, with true anomaly increasing counterclockwise. The scale is in kilometers.

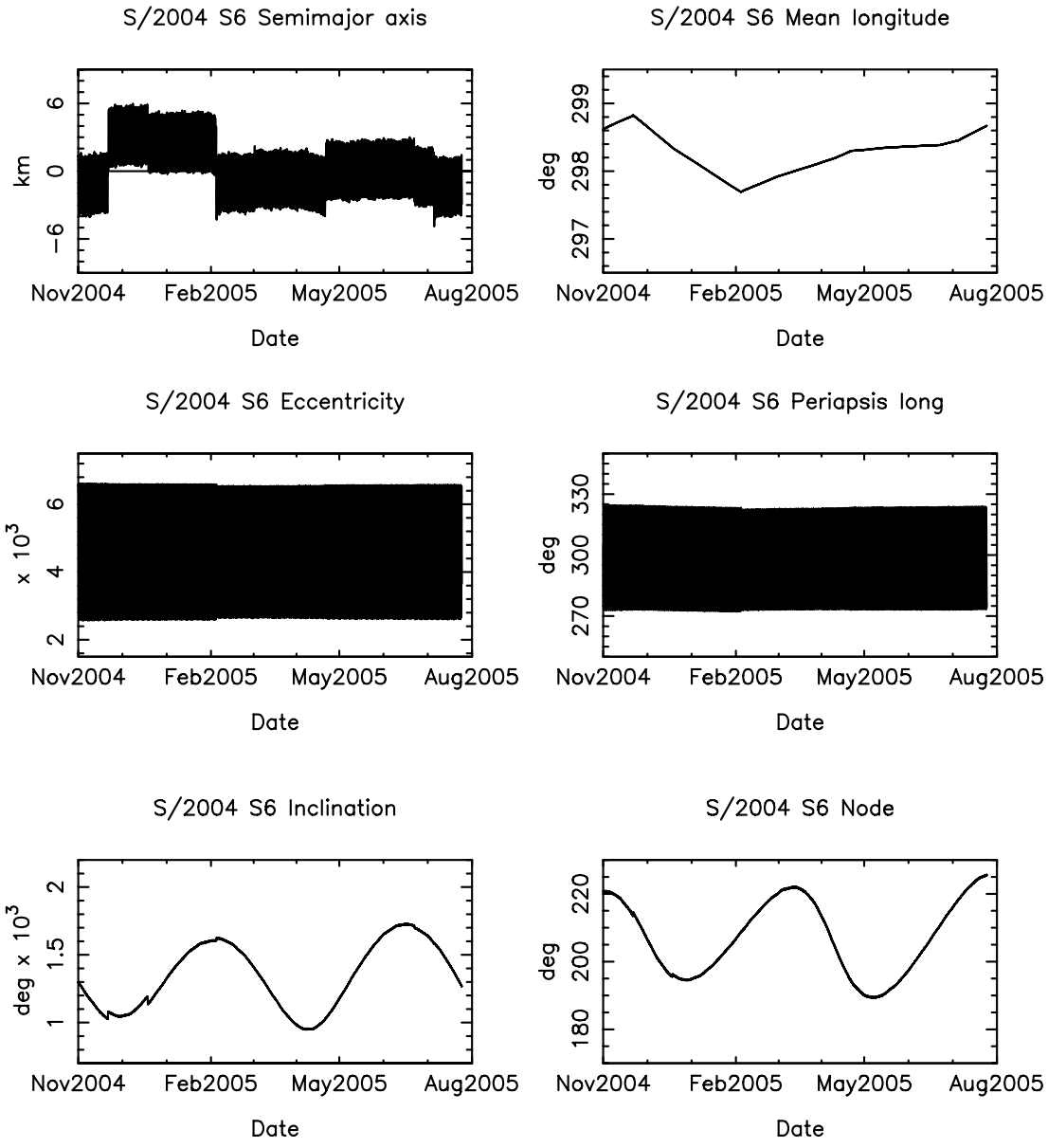

FIG. 16.—Osculating elements for the orbit integration of S/2004 S6, assuming that it reappears as C11, C13, C20, and C21. The secular rates have been removed from the mean longitude, periapse longitude, and node.

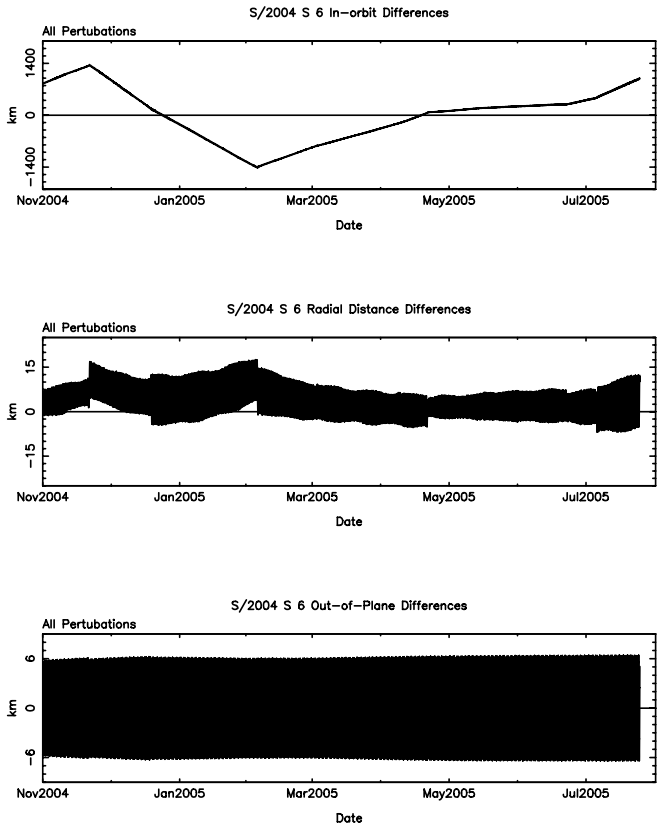

FIG. 17.—Differences between the integrated orbit and the mean precessing ellipse for S/2004 S6/C13/C20/C21.

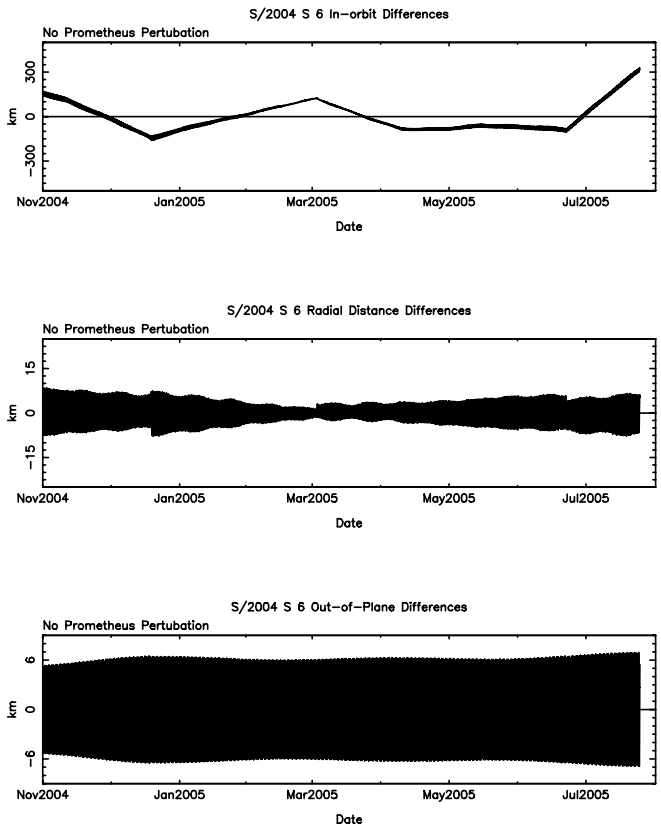

FIG. 18.—Differences between the integrated orbit and the mean precessing ellipse for S/2004 S6/C13/C20/C21 with Prometheus perturbations excluded.

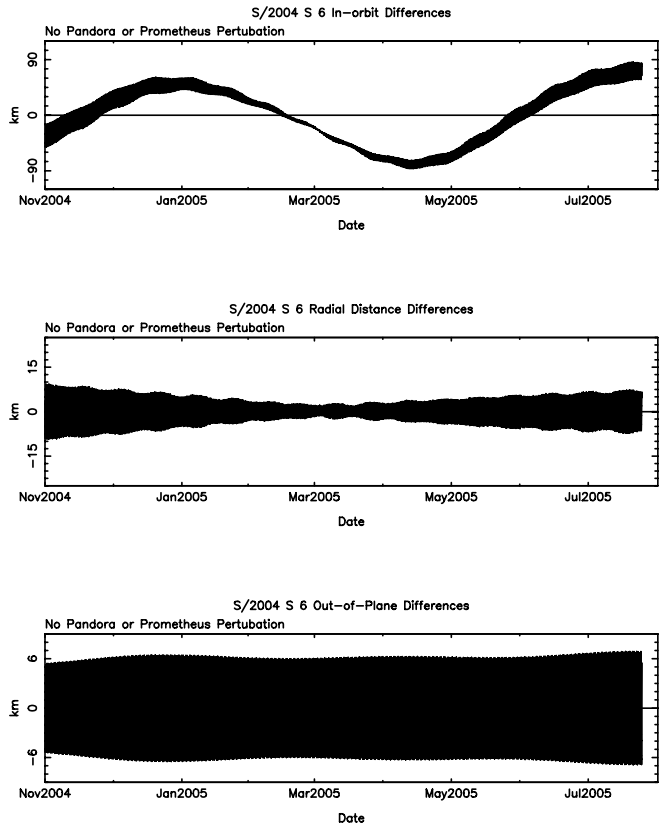

FIG. 19.—Differences between the integrated orbit and the mean precessing ellipse for S/2004 S6/C13/C20/C21 with Prometheus and Pandora perturbations excluded.

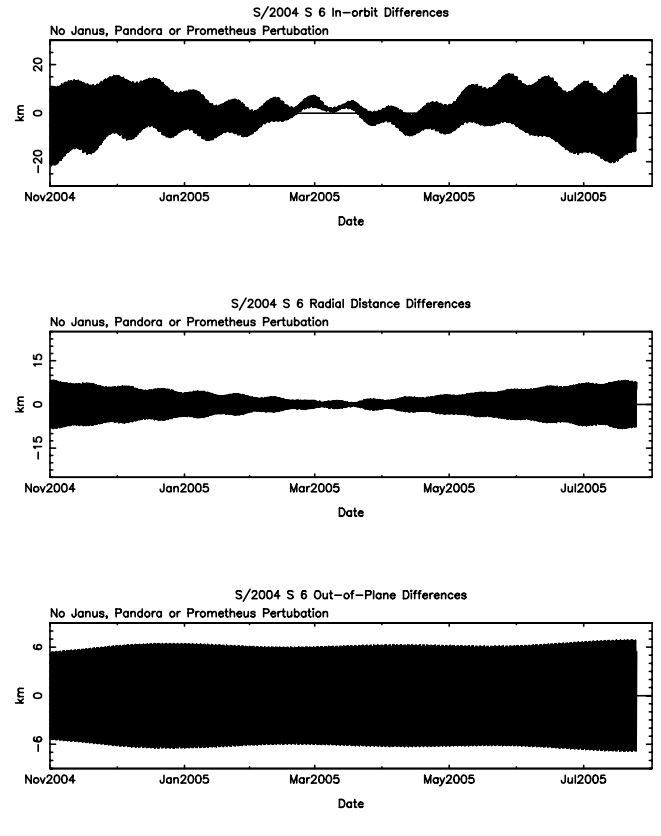

FIG. 20.—Differences between the integrated orbit and the mean precessing ellipse for S/2004 S6/C13/C20/C21 with Prometheus, Pandora, and Janus perturbations excluded.

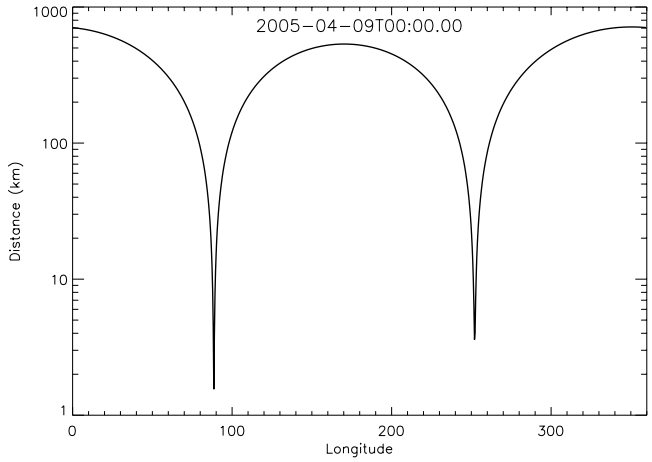

FIG. 21.—Distance between the S/2004 S6/C13/C20/C21 orbit and the core of the F ring on 2005 April 9.

If the above associations are real, then it suggests that these bodies are solid satellites instead of transient "clumps" (Poulet et al. 2000; Barbara & Esposito 2002), whose lifetimes are expected to be less than a few months. Moreover, both orbit solutions cross the core of the F ring, in a radial sense. The nodal rates are highly uncertain, but if they precess at different rates than the node of the F ring, then both orbits must periodically intersect the F-ring core.[6] As seen in Figure 21, S6's orbit came within about 1.5 km of the F-ring core, less than its estimated vertical thickness (Bosh et al. 2002), in 2005 April. It would be surprising if such an interaction resulted in no observable consequences; indeed, Charnoz et al. (2005) suggest that a newly discovered spiral structure observed in the tenuous material surrounding the F ring may be among those consequences. Differential precession of the node would also imply that the orbits of S/2004 S6 and S/2004 S3 must periodically intersect one another. If both bodies are permanent satellites, then they may be protected by some mutual interaction.

To summarize: based on orbit fits, S/2004 S3 and S6 may have been observed over the course about 1 yr, suggesting that they are not simply transient clumps. Radiometric arguments, on the other hand, suggest that the bodies did not actually exist by the time of 2004 November 15, so they may in fact have been transient clumps. Only S/2004 S6 has an alibi to explain its absence on 2004 November 15; S/2004 S3 does not, so it seems likely that the association between the observations S/2004 S3, C12, and C22 is a coincidence.[7]

We acknowledge the *Cassini* Imaging Science Team; in particular, the CICLOPS group at the Space Science Institute in Boulder, Colorado, and Carl Murray and the group at Queen Mary, University of London, in the planning and execution of imaging observations of the small satellites. We also acknowledge Emma Birath of CICLOPS/SSI for her work in determining the point-spread function of the *Cassini* cameras. We thank Bob Gaskell for his help with the *Voyager* image geometry, which was necessary for confirming our identification of S/1981 S14 as Pallene. Some satellite measurements were provided by the *Cassini* navigation team. We thank Sebastien Charnoz for discussions in the initial stages of this work. This work was funded by the *Cassini* project and NASA PGG grant NAGW 11641.

[6] As long as the node and apse of the orbit precess at different rates, the ascending node of the orbit on the plane of the F ring must periodically point along the longitude at which the orbit and the F ring have the same radius.

[7] The association between S/2004 S3 and S/2004 S4 may, of course, still be real.

REFERENCES

Acton, C. H. 1996, Planet. Space Sci., 44, 65
Barbara, J. M., & Esposito, L. W. 2002, Icarus, 160, 161
Borderies, N., Goldreich, P., & Tremaine, S. 1984, in Planetary Rings, ed. R. Greenberg & A. Brahic (Tucson: Univ. Arizona Press), 713
Bosh, A. S., Olkin, C. B., French, R. G., & Nicholson, P. D. 2002, Icarus, 157, 57
Broucke, R. A., & Cefola, P. J. 1972, Celest. Mech., 5, 303
Charnoz, S., Porco, C. C., Déau, E., Brahic, A., Spitale, J. N., Bacques, G., & Baillie, K. 2005, Science, 310, 1300
Cuzzi, J. N., & Scargle, J. D. 1985, ApJ, 292, 276
Danielson, G. E., Kupferman, P. N., Johnson, T. V., & Soderblom, L. A. 1981, J. Geophys. Res., 86, 8683
Dollfus, A., & Brunier, S. 1981, Icarus, 48, 29
French, R. G., & McGhee, C. A. 2004, BAAS, 36, 859
French, R. G., McGhee, C. A., Dones, L., & Lissauer, J. L. 2003, Icarus, 162, 143
French, R. G., McGhee, C. A., Frey, M., Hock, R., Rounds, S., Jacobson, A., & Verbiscer, A. 2006, PASP, 118, 246
Goldreich, P., & Rappaport, N. 2003, Icarus, 166, 320
Gordon, M. K., Murray, C. D., & Beurle, K. 1996, Icarus, 121, 114
Jacobson, R. A. 1991, A&AS, 90, 541
———. 1996, BAAS, 28, 1185
Jacobson, R. A., & French, R. G. 2004, Icarus, 172, 382
Jacobson, R. A., Spitale, J. N., Porco, C. C., & Owen, W. M., Jr. 2006, AJ, 132, 711
Jacobson, R. A., et al. 2005, BAAS, 37, 729
McGhee, C. A. 2000, Ph.D. thesis, Cornell Univ.
McGhee, C. A., Nicholson, P. D., French, R. D., & Hall, K. J. 2001, Icarus, 152, 282
Murray, C. D., Cooper, N. J., Evans, M. W., & Beurle, K. 2005, Icarus, 179, 222
Nicholson, P. D., Hamilton, D. P., Matthews, K., & Yoder, C. F. 1992, Icarus, 100, 464
Null, G. W., Lau, E. L., Biller, E. D., & Anderson, J. D. 1981, AJ, 86, 456
Porco, C. C. 2004a, IAU Circ. 8389
———. 2004b, IAU Circ. 8401
———. 2004c, IAU Circ. 8432
———. 2005, IAU Circ. 8524
Porco, C. C., et al. 2004, Space Sci. Rev., 115, 363
———. 2005, Science, 307, 1226
Poulet, F., Sicardy, B., Nicholson, P. D., Karkoschka, E., & Caldwell, J. 2000, Icarus, 144, 135
Press, W. H., Teukolsky, S. A., Vetterling, W. T., & Flannery, B. P. 1992, Numerical Recipes in C (2nd ed.; New York: Cambridge Univ. Press)
Renner, S., Sicardy, B., & French, R. G. 2005, Icarus, 174, 230
Rosen, R. A., Tyler, G. L., Marouf, E. A., & Lissauer, J. L. 1991, Icarus, 93, 25
Seidelmann, P. K., Harrington, R. S., Pascu, D., Baum, W. A., Currie, D. G., Westphal, J. A., & Danielson, G. E. 1981, Icarus, 47, 282
Sharringhausen, B. R., Nicholson, P. D., Brandl, B., Hayward, T. L., Dekany, R., Troy, G. M., & Bloemhof, E. E. 2003, Icarus, 162, 385
Showalter, M. R. 1991, Nature, 351, 709
Standish, E. M. 2003, Jet Propulsion Laboratory Internal Document IOM 312.N-03-24 (Pasadena: JPL)
Synnott, S. P. 1986, Icarus, 67, 189
Yoder, C. F., Columbo, G., Synnott, S. P., & Yoder, K. A. 1983, Icarus, 53, 431
Yoder, C. F., Synnott, S. P., & Salo, H. 1989, AJ, 98, 1875